REPORT DOCUMENTATION PAGE

Form Approved OMB NO. 0704-0188

1. REPORT DATE (DD-MM-YYYY)	2. REPORT TYPE	3. DATES COVERED (From - To)
01-09-2021	Final Report	15-Jul-2016 - 14-Jan-2021

4. TITLE AND SUBTITLE
Final Report: Elucidating Correlation of Morphology with Charge Transport in Polymerized Ionic Liquids

5a. CONTRACT NUMBER
W911NF-16-1-0402

5b. GRANT NUMBER

5c. PROGRAM ELEMENT NUMBER
611102

6. AUTHORS

5d. PROJECT NUMBER

5e. TASK NUMBER

5f. WORK UNIT NUMBER

7. PERFORMING ORGANIZATION NAMES AND ADDRESSES
University of Tennessee at Knoxville
Office of Sponsored Programs
1534 White Avenue
Knoxville, TN 37996 -1529

8. PERFORMING ORGANIZATION REPORT NUMBER

9. SPONSORING/MONITORING AGENCY NAME(S) AND ADDRESS (ES)
U.S. Army Research Office
P.O. Box 12211
Research Triangle Park, NC 27709-2211

10. SPONSOR/MONITOR'S ACRONYM(S)
ARO

11. SPONSOR/MONITOR'S REPORT NUMBER(S)
67802-CH.4

12. DISTRIBUTION AVAILIBILITY STATEMENT
Approved for public release; distribution is unlimited.

13. SUPPLEMENTARY NOTES
The views, opinions and/or findings contained in this report are those of the author(s) and should not contrued as an official Department of the Army position, policy or decision, unless so designated by other documentation.

14. ABSTRACT

15. SUBJECT TERMS

16. SECURITY CLASSIFICATION OF:			17. LIMITATION OF ABSTRACT	15. NUMBER OF PAGES	19a. NAME OF RESPONSIBLE PERSON
a. REPORT	b. ABSTRACT	c. THIS PAGE			STEPHEN PADDISON
UU	UU	UU	UU		19b. TELEPHONE NUMBER +18-659-7420

RPPR Final Report
as of 08-Sep-2021

Agency Code: 21XD

Proposal Number: 67802CH **Agreement Number: W911NF-16-1-0402**
INVESTIGATOR(S):

Name: STEPHEN J. PADDISON Ph.D.
Email: spaddison@utk.edu
Phone Number: +18659742026
Principal: Y

Organization: **University of Tennessee at Knoxville**
Address: Office of Sponsored Programs, Knoxville, TN 379961529
Country: USA
DUNS Number: 003387891 EIN: 626001636
Report Date: 14-Apr-2021 Date Received: 01-Sep-2021
Final Report for Period Beginning 15-Jul-2016 and Ending 14-Jan-2021
Title: Elucidating Correlation of Morphology with Charge Transport in Polymerized Ionic Liquids
Begin Performance Period: 15-Jul-2016 **End Performance Period:** 14-Jan-2021
Report Term: 0-Other
Submitted By: STEPHEN PADDISON Email: spaddison@utk.edu
Phone: (+18) 659-742026

STEM Degrees: 1 **STEM Participants:**

Major Goals: To determine the impact of the chemical composition of aromatic and alkyl cations with distinct anions on the mesoscale morphology and conductive behavior of polymerized ionic liquids (polyILs).
- To investigate the pendant alkyl chain length effect on morphology of polyILs;
- To characterize the structure of polyILs with both X-ray scattering and neutron scattering;
- To study the anion effect on morphology of polyILs;
- To investigate the effect of functional group of polycation (imidazolium versus ammonium) on morphology of polyILs;
- To investigate the position effect of functional group (near the backbone, away the backbone and in the backbone);
- To explore the underlying mechanisms of ion transport in polyILs.
- To study the anion effect on ion transport mechanism of polyILs;
- To investigate the effect of functional group of polycation (imidazolium versus ammonium) on ion transport mechanism of polyILs; To investigate the pendant alkyl chain length effect on ion transport mechanism of polyILs;
- To investigate the pendant alkyl chain length effect on ion transport mechanism of polyILs

Accomplishments: • Simulated a related set of polyILs with properly derived all-atom force field.
- Performed detailed structural analysis on simulation trajectories. The X-ray and neutron scattering structure factors were computed for the entire homologous series of polyILs.
- Derived an analysis scheme to assess ionic cluster formation and connectivity.
- Developed a novel scheme elucidate the ion hopping mechanism in polyILs.
- Applied the methodology to study the effects of different anions, cationic groups and pendant alkyl chains.

Training Opportunities: Nothing to Report

Results Dissemination: Nothing to Report

Honors and Awards: Reappointed the Gibson Endowed Professor of Engineering for another 5 years (2019-2024).

Protocol Activity Status:

Technology Transfer: Nothing to Report

RPPR Final Report
as of 08-Sep-2021

PARTICIPANTS:

Participant Type: PD/PI
Participant: Stephen Paddison
Person Months Worked: 12.00 **Funding Support:**
Project Contribution:
National Academy Member: N

Participant Type: Graduate Student (research assistant)
Participant: Xubo Luo
Person Months Worked: 12.00 **Funding Support:**
Project Contribution:
National Academy Member: N

Participant Type: Postdoctoral (scholar, fellow or other postdoctoral position)
Participant: Hongjun Liu
Person Months Worked: 1.00 **Funding Support:**
Project Contribution:
National Academy Member: N

ARTICLES:

Publication Type: Journal Article Peer Reviewed: Y **Publication Status:** 1-Published
Journal: Macromolecules
Publication Identifier Type: DOI Publication Identifier: 10.1021/acs.macromol.6b02708
Volume: 50 Issue: 7 First Page #: 2889
Date Submitted: 8/30/17 12:00AM Date Published: 3/1/17 5:00AM
Publication Location:
Article Title: Alkyl Chain Length Dependence of Backbone-to-Backbone Distance in Polymerized Ionic Liquids: An Atomistic Simulation Perspective on Scattering
Authors: Hongjun Liu, Stephen J. Paddison
Keywords: polyILs, atomistic MD simulations, neutron scattering, X-ray scattering
Abstract: The backbone-to-backbone correlation length in polymerized ionic liquids (polyILs) manifested as the low-q peak in scattering profiles increases with increasing alkyl chain length, concomitant with ever-growing nonpolar domain size. Understanding the dependence of the correlation length on the pendant alkyl chain length is crucial to effectively designing polyILs for electrochemical applications. Herein, extensive atomistic MD simulations for a complete homologous series of poly(n-alkylvinylimidazolium bis(trifluoromethylsulfonyl)-imide), poly(CnVim Tf2N) (n = 2?8), have been carried out to investigate the liquid structure with emphasis on scattering. Neutron scattering with isotopic labeling affords more versatile ways to vet the intrinsic structure, but different isotopically labeled neutron and X-ray scattering data do not necessarily lead to the same position of the low-q peaks. Such an unintended consequence has a nontrivial implication on exploitation of scattering experiments
Distribution Statement: 3-Distribution authorized to U.S. Government Agencies and their contractors
Acknowledged Federal Support: **Y**

RPPR Final Report
as of 08-Sep-2021

Publication Type: Journal Article Peer Reviewed: Y **Publication Status:** 1-Published
Journal: ACS Macro Letters
Publication Identifier Type: DOI Publication Identifier: 10.1021/acsmacrolett.7b00335
Volume: 6 Issue: First Page #: 941
Date Submitted: 8/30/17 12:00AM Date Published: 8/1/17 4:00AM
Publication Location:
Article Title: Polymerized Ionic Liquids: Correlation of Ionic Conductivity with Nanoscale Morphology and Counterion Volume
Authors: Ciprian Iacob, Atsushi Matsumoto, Marissa Brennan, Hongjun Liu, Stephen J. Paddison, Osamu Urakav
Keywords: broadband dielectric spectroscopy, molecular dynamics simulations, morphology, ionic conductivity, Tg
Abstract: The impact of the chemical structure on ion transport, nanoscale morphology, and dynamics in polymerized imidazolium-based ionic liquids is investigated by broadband dielectric spectroscopy and X-ray scattering, complemented with atomistic molecular dynamics simulations. Anion volume is found to correlate strongly with Tg independent ionic conductivities spanning more than 3 orders of magnitude. In addition, a systematic increase in alkyl side chain length results in about one decade decrease in Tg-independent ionic conductivity correlating with an increase in the characteristic backbone-to-backbone distances found from scattering and simulations. The quantitative comparison between ion sizes, morphology, and ionic conductivity underscores the need for polymerized ionic liquids with small counterions and short alkyl side chain length in order to obtain polymer electrolytes with higher ionic conductivity
Distribution Statement: 3-Distribution authorized to U.S. Government Agencies and their contractors
Acknowledged Federal Support: **Y**

Publication Type: Journal Article Peer Reviewed: Y **Publication Status:** 1-Published
Journal: Electrochimica Acta
Publication Identifier Type: DOI Publication Identifier: 10.1016/j.electacta.2017.06.089
Volume: 246 Issue: First Page #: 914
Date Submitted: 8/31/17 12:00AM Date Published: 8/1/17 4:00AM
Publication Location:
Article Title: Three-dimensional Catenated 1-ethyl-3-methylimidazolium Halotitanate Ionic Liquid Electrolytes for Electrochemical Applications
Authors: Gioele Pagot, Federico Bertasi, Keti Vezzù, Fatemeh Sepehr, Xubo Luo, Graeme Nawn, Enrico Negro,
Keywords: Ionic liquid electrolytes Mg-Ti alloy electrodeposition 3D-catenated structure density functional theory conductivity mec
Abstract: A new family of ionic liquid based electrolytes ([EMImCl/(TiCl4)1.4]/(d-MgCl2)x) for electrochemical applications is proposed. These materials are obtained by direct reaction of 1-ethyl-3-methylimida- zolium chloride (EMImCl) with titanium(IV) chloride (TiCl4), and doped with increasing amounts of d-MgCl2. Modulated differential scanning calorimetry (MDSC) measurements show that in these electrolytes the glass transition temperature, Tg, occurs at ┌36 C, and that the crystallization and melting transitions are inhibited by the presence of large and highly amorphous charge delocalized anionic domains. Vibrational studies indicate that in the electrolyte the anionic domains consist of large monomeric and dimeric 3D-catenated halotitanate clusters, in which magnesium chloride units are coordinated to Ti species, and whose equilibrium concentration is modulated by the concentration of d-MgCl2. Density functional theory (DFT) based electronic structure calculations were undertaken to underst
Distribution Statement: 3-Distribution authorized to U.S. Government Agencies and their contractors
Acknowledged Federal Support: **Y**

RPPR Final Report
as of 08-Sep-2021

Partners

,

Alexei Sokolov, ORNLVito Di Noto, University of Padova, Italy

I certify that the information in the report is complete and accurate:
Signature: Stephen Paddison
Signature Date: 9/1/21 6:33PM

Project Summary- Grant # W911NF-16-1-0402

(Reporting Period: July 2016 – January 2021)

Effort Title: Elucidating Correlation of Molecular Structure with Charge Transport in Polymerized Ionic Liquids

Stephen J. Paddison
Department of Chemical and Biomolecular Engineering
University of Tennessee, Knoxville, TN, 37996

Objective

To determine the impact of the chemical composition of aromatic and alkyl cations with distinct anions on the mesoscale morphology and conductive behavior of polymerized ionic liquids (polyILs).

Approach

- To investigate the pendant alkyl chain length effect on morphology of polyILs;
- To characterize the structure of polyILs with both X-ray scattering and neutron scattering;
- To study the anion effect on morphology of polyILs;
- To investigate the effect of functional group of polycation (imidazolium versus ammonium) on morphology of polyILs;
- To investigate the position effect of functional group (near the backbone, away the backbone and in the backbone);
- To explore the underlying mechanisms of ion transport in polyILs.
- To study the anion effect on ion transport mechanism of polyILs;
- To investigate the effect of functional group of polycation (imidazolium versus ammonium) on ion transport mechanism of polyILs; To investigate the pendant alkyl chain length effect on ion transport mechanism of polyILs;
- To investigate the pendant alkyl chain length effect on ion transport mechanism of polyILs;

Relevance to Army

The fundamental understanding gained from this project will provide the scientific basis for deliberate and optimal design of polymerized ionic liquids for applications in dye-sensitized solar cells, lithium batteries, actuators, field-effect transistors, light emitting electrochemical cells, and electrochromic devices. It is also envisaged that the information regarding the interplay between molecular structure and ion transport in polymerized ionic liquids gained from this work will be of immediate benefit to the U.S. Army as well as the larger polymer science scientific communities.

Accomplishments for Reporting Period

- Simulated a related set of polyILs with properly derived all-atom force field.
- Performed detailed structural analysis on simulation trajectories. The X-ray and neutron scattering structure factors were computed for the entire homologous series of polyILs.
- Derived an analysis scheme to assess ionic cluster formation and connectivity.
- Developed a novel scheme elucidate the ion hopping mechanism in polyILs.
- Applied the methodology to study the effects of different anions, cationic groups and pendant alkyl chains.

Collaborations and Technology Transfer

- Dr. David Salas-de la Cruz & Prof. Karen Winey, (Univ. Penn): prior state of the art experimental work (X-ray scattering and interpretation)
- Dr. Ciprian Iacob & Prof. James Runt (Penn State Univ.): X-ray scattering data of polyILs.
- Dr. Federico Bertasi & Prof. Vito Di Noto (Univ. Padova, Italy): preparation of salts + polyILs, far-IR spectroscopy.
- Dr. Sara Cavaliere, Dr. Deborah J. Jones, & Prof. Jacques Rozière (University of Montpellier), experimental results of PFSAs and blends.
- Dr. Alexei Sokolov, Oak Ridge National Laboratory/UTK, BDS, DSC, and NMR of polyILs.

Resulting Journal Publications During Reporting Period

- Liu, H; Paddison, S.J, Alkyl Chain Length Dependence of Backbone-to-Backbone Distance in Polymerized Ionic Liquids: An Atomistic Simulation Perspective on Scattering. *Macromolecules* **2017** 50, 2889-2895.

- Iacob, C.; Matsumoto, A.; Brennan, M.; Liu, H.; Paddison, S.J; Urakawa, O.; Inoue, T.; Sangoro, J; Runt, J., Polymerized Ionic Liquids: Correlation of Ionic Conductivity with Nanoscale Morphology and Counterion Volume, *ACS Macro Letters* **2017**, 6, 941-946.
- Pagot, G.; Bertasi, F.; Vezzù, K.; Sepehr, F.; Luo, X.; Nawn, G.; Negro, E.; Paddison, S. J.; Di Noto, V. Three-dimensional Catenated 1-ethyl-3-methylimidazolium Halotitanate Ionic Liquid Electrolytes for Electrochemical Applications. *Electrochimica Acta* **2017**, 246, 914-923.
- Liu, H.; Cavaliere, S.; Jones, D. J.; Rozière, J.; Paddison, S. J., Scaling Behavior of Nafion with Different Model Parameterizations in Dissipative Particle Dynamics Simulations. *Macromolecular Theory and Simulations* **2018**, 27, 180000.
- Liu, H.; Cavaliere, S.; Jones, D. J.; Rozière, J.; Paddison, S. J., Morphology of Hydrated Nafion through a Quantitative Cluster Analysis: A Case Study Based on Dissipative Particle Dynamics. *Journal of Physical Chemistry C* **2018**, 122, 13130-13139.
- Heres, M.; Cosby, T.; Mapesa, E. U.; Liu, H.; Berdzinski, S.; Strehmel, V.; Dadmun, M.; Paddison, S. J.; Sangoro, J., Ion Transport in Glassy Polymerized Ionic Liquids: Unraveling the Impact of the Molecular Structure. *Macromolecules* **2019**, 52, 88−95.
- Luo, X.; Liu, H.; Bae, C.; Tuckerman, M. E.; Hickner, M. A.; Paddison, S. J., Mesoscale Simulations of Quaternary Ammonium-Tethered Triblock Copolymers: Effects of the Degree of Functionalization and Styrene Content. *J. Phys. Chem. C* **2020**, 124, 16315–16323.
- Luo, X.; Liu, H.; and Paddison, S. J. Molecular dynamics simulations of polymerized ionic liquids: mechanism of ion transport for different anions, *ACS Applied Polymer Materials* **2021**, 3, 141-152.
- Liu, H.; Luo, X.; Sokolov, A.; and Paddison, S. J. Quantitative evidence of mobile ion hopping in polymerized ionic liquids*, Journal of Physical Chemistry B* **2021**, 125, 372-381. L. R. Pratt Festschrift.
- Zhu, Z. and Paddison, S.J. Morphology and Ion Transport in Ion-containing Polymers, *Journal of Physical Chemistry B* **2021**, invited Perspective Article, under review.

Graduate Students Involved During Reporting Period

- Xubo Luo (Ph.D.)

Awards, Honors and Appointments

- Reappointed the *Gibson Endowed Professor of Engineering* for another 5 years (2019-2024).

A complete set of the simulation and analysis methods have been sorted out to study the structural properties and ion transport mechanism of polyILs. The methods were applied to a variety of molecular structures to seek for the design rules of polyILs. The simulated materials, which are listed in Table 1, have different counterions and ionic monomers, which provide sufficient coverage to study the effect of counterion, the linker between the polymer backbone and the ionic head group, and the pendant tail at the open end. The common polycation, poly(ethyl vinyl imidazolium), namely Poly(C_2VIm), was paired with four different counterions, which varied from the monatomic anion of bromide to the large polyatomic anion of bis(trifluoromethane)sulfonimide (Tf_2N). poly(C_nMTMA) at 400K with different pendant tails.

Each simulated system consisted of 10 40-mer polycations and 400 anions. All molecular dynamics (MD) simulations were carried out with the GROMACS package using the general AMBER force field all-atom parameters following an established procedure.[1,2] Tf_2N^- had multiple conformations so that two charge models were developed for this anion based on cis and trans conformations, which were named 'Tf_2N^-_1' and 'Tf_2N^-_2', respectively.[3] For each system, a variety of temperatures were simulated. Simulations were firstly running in NpT ensemble to obtain the density. Bussi stochastic thermostat was used to control temperature, while a Berendsen barostat followed by a Parrinello-Rahman barostat were used to control pressure at 1 atm. NVT ensemble productions were performed at the desired density estimated by NpT ensemble. The system was equilibrated for at least 20 ns. Typically, trajectories were saved every 10ps for 50ns and every 100ps for 300 ns, respectively, to ensure the enough long trajectories and simultaneously control the size of the data file. Finer time intervals of trajectory were used when required in analysis.

Table 1. Simulated materials

Variable	Materials

Anion	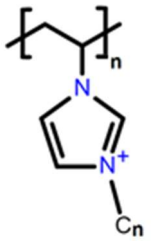 Poly(C_nVIm)	Br^-	BF_4^-	PF_6^-	Tf_2N^-
Cationic group	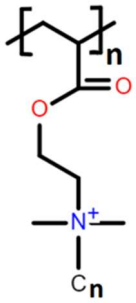 Poly(C_nMTMA)	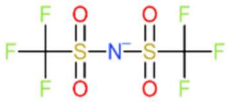			(Tf_2N^-)

The structure factors were firstly calculated for the structure properties and the comparison with the experimental data. Both the direct and Fourier transform methods can be applied to calculate the structure factors of the polyILs. In this research, partial structure factor was estimated by Fourier transformation of $g(r)$:

$$S_{\alpha\beta}(q) = x_\alpha \delta_{\alpha\beta} + x_\alpha x_\beta \rho_0 \int_0^{L/2} 4\pi r^2 [g_{\alpha\beta}(r) - 1] \frac{sin(qr)}{qr} w(r) dr$$

where $\delta_{\alpha\beta}$ is the Kronecker delta. x_α is the corresponding mole fraction of α and ρ_0 is the total number density of the system. The revised Lorch window function, $w(r) = 3/(2\pi r/L)^3$ [$\sin(2\pi r/L) - 2\pi r/L \cos(2\pi r/L)$], was applied to remedy the cutoff ripple artifact. For X-ray scattering, partial structure factors were weighted with the atomic form factors leading to the total X-ray structure factor:

$$S^X(q) = \frac{1}{\sum_\alpha x_\alpha f_\alpha^2} \sum_\alpha^n \sum_\beta^n f_\alpha(q) f_\beta(q) S_{\alpha\beta}(q)$$

where $f_\alpha(q)$ represents the X-ray atomic form factor of α and can be approximated with a series of Gaussian functions of q over the range of (0, 25) $Å^{-1}$ according to:

$$f_\alpha = \sum_{i=1}^{4} a_i \, exp[-b_i (q/4\pi)^2] + c$$

The tabulated coefficients a_i, b_i, and c are reported in Table 6.1.1.4 of the International Tables for Crystallography. For neutron scattering, $f_\alpha(q)$ is replaced with the neutron scattering lengths, b_α: -3.739, 5.803, 6.646, 9.36, 5.654, 6.671 and 2.847 fm for hydrogen, oxygen, carbon, nitrogen, fluorine, deuterium and sulfur, respectively. Hence, the total neutron structure factor is:

$$S^N(q) = \frac{1}{\sum_\alpha x_\alpha \, b_\alpha^2} \sum_\alpha^n \sum_\beta^n b_\alpha \, b_\beta S_{\alpha\beta}(q)$$

The structure factors of a complete homologous series of 7 poly(C_n VIm Tf2N) present a clear trend on the effect of alkyl chain length. Simulated X-ray structure factors of poly(C_n VIm Tf2N) as a function of alkyl chain length are compared with recent experiments in Figure 1. The homologous series of poly(C_n VIm Tf_2N) shows three characteristic intermolecular features below 2 $Å^{-1}$. The low-q peaks are taken to be the backbone-to-backbone peak (q_b) or polarity peak, the intermediate-q peaks are denoted as the ionic peak (q_i , correlation between anions) or charge peak, and the high-q peaks as the pendant-to-pendant peak (q_p , correlation between pendant groups of the polycation) or adjacency peak. Three characteristic peaks are well reproduced by the atomistic simulations, and the trends are strikingly similar to the experimental results. The most conspicuous feature in Figure 1 is that the low-q peak shifts to lower q with stronger intensity as the alkyl chain length increases, indicating an increase in backbone-to-backbone separation and the concomitant growth of the nonpolar nanodomains. Though it appears poly(C_2Vim Tf_2N) is an outlier whose low-q peak position is somehow lower than expected, such a deviation is not observed in the various structure factors as demonstrated below. The low-q peak is insignificant compared with the other two scattering peaks in poly(C_2Vim Tf_2N) and becomes comparable in intensity when n = 4 or 5 and much more dominant in poly(C_nVim Tf_2N) with longer alkyl chains (n > 5). In contrast to qb, there is no substantial q shift observed in qi and q_p : q_i slightly shifts to lower q with weaker intensity, while there is very little shift in q_p, but with stronger intensity as the alkyl chain becomes longer. The weaker correlation and slightly larger separation between anions with increasing alkyl chain length are because the ionic separation must increase to accommodate progressively larger nonpolar domains. The adjacency or direct contact distance is hardly affected by the nonpolar domains as there is no shift in the position of q_p.

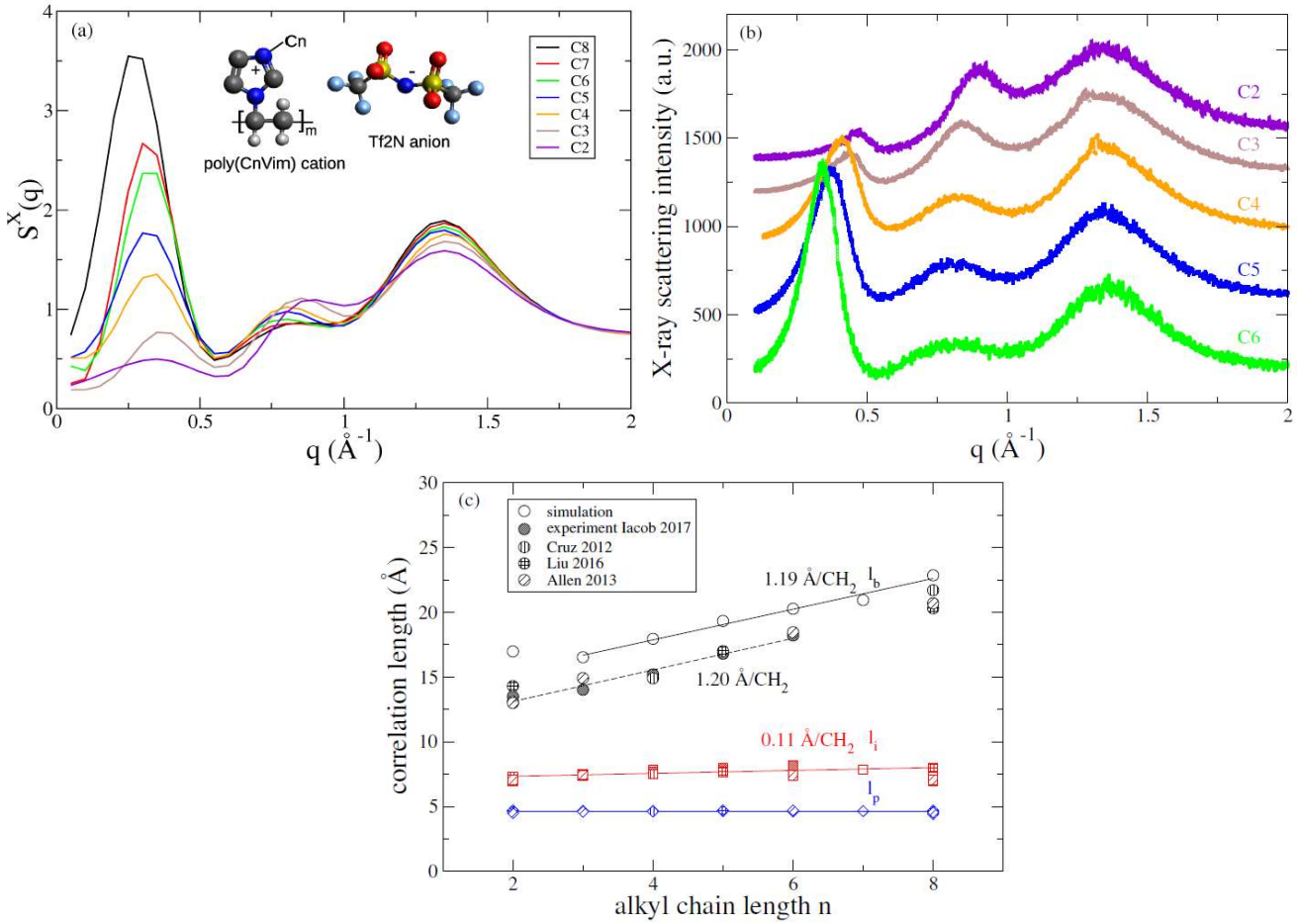

Figure 1. (a) Simulated total X-ray structure factors with an inset of the schematic structure of poly(C_nVim Tf_2N) and (b) experimental X-ray scattering profiles of poly(C_nVim Tf_2N). (c) Correlation lengths derived from X-ray scattering peak positions of poly(C_nVim Tf_2N) as a function of alkyl chain length in comparison with previous experimental values and simulation. The solid lines are the least-squares fits of the simulated data, and the dashed line the experimental results. The error bars are smaller than the symbol size. l_b, l_i, and l_p are the backbone-to-backbone correlation length, ionic correlation length, and pendant-to-pendant correlation length, respectively.

Correlation lengths derived from peak positions in $S^X(q)$ of poly(C_n VIm Tf_2N) as a function of alkyl chain length are presented in Figure 1(c). The overall agreement between simulation and experiment is satisfactory. The correlation length, lp, remains a constant 4.7 Å regardless of n, while l_i around 7.6 Å increases slightly with n. The simulated correlation length, l_b, significantly overestimates the experimental scale, but both increase linearly with n at a similar rate of 1.19 Å/CH_2 (simulation) vs 1.20 Å/CH_2 (experiment). The direct manifestation of backbone-to-backbone correlation length through analysis of alkyl chain extension also leads to a slope of about

1.1 Å/CH_2, corroborating the scattering findings. These estimates are lower than the experimental rate of 1.5 Å/CH_2 (n = 2, 4, and 8) and 1.3 Å/CH_2 (n = 2, 3, 6, and 8) and are higher than that of our recent simulation (1.0 Å/CH_2 for n = 2, 5, and 8). The low-q peaks have been identified as a signature feature of nanoscale aggregation in both polymers and molecular ionic liquids. Our estimate is generally consistent with the experimental values ranging from 1.0 to 2.3 Å/CH_2 in side-chain polymers and various ILs. The overestimated lb can be attributed to the downward shift in the low-q peaks at higher temperatures due to thermal expansion. Simulations were run at an elevated temperature (i.e., 400 K) to greatly improve the sampling quality of the configuration space, while the X-ray scattering experiments were measured at room temperature of 298 K.

Complementary to the X-ray scattering profiles, we also report simulated neutron scattering data for the series of poly(C_nVim Tf_2N) using hydrogen/deuterium substitution to further investigate the contributions of the various components to the total scattering. Selective isotopic labeling in neutron scattering provides a molecular level resolution and is essential for an in-depth understanding of the atomistic structure of polyILs. The total neutron scattering factors for the fully protiated, perdeuterated, backbone deuterated, and alkyl chain deuterated of 3 poly(C_nVIm Tf_2N) are presented in Figure 2. The neutron scattering profiles markedly depend on the isotopic substitution pattern. For the fully protiated, perdeuterated, and alkyl chain deuterated samples, the low-q peak is relatively small, whereas in the backbone deuterated samples, it is much more intense and becomes the most dominant contribution to the overall scattering. The backbone deuterated polyILs samples should be among the best choices for experimentalists to exploit the capacity of SANS for quality signal in terms of the low-q scattering peak. Although all neutron or X-ray scattering of each poly(C_n Vim Tf_2N) is vetting the very same intrinsic structure, complications from weighted individual partial structure factors by scattering lengths or form factors make identification of a unique peak nearly impossible. The X-ray scattering and distinct isotopic labeled neutron scattering data do not necessarily lead to the characteristic peaks with the same positions. Our simulations of the shorter alkyl chain (C3) or longer chain (C7) result in a more consistent estimate of the low-q positions than that of its intermediate counterpart (C5). It is advised to pay extra heed to comparison of correlation lengths derived from different scattering implementations of the same compound.

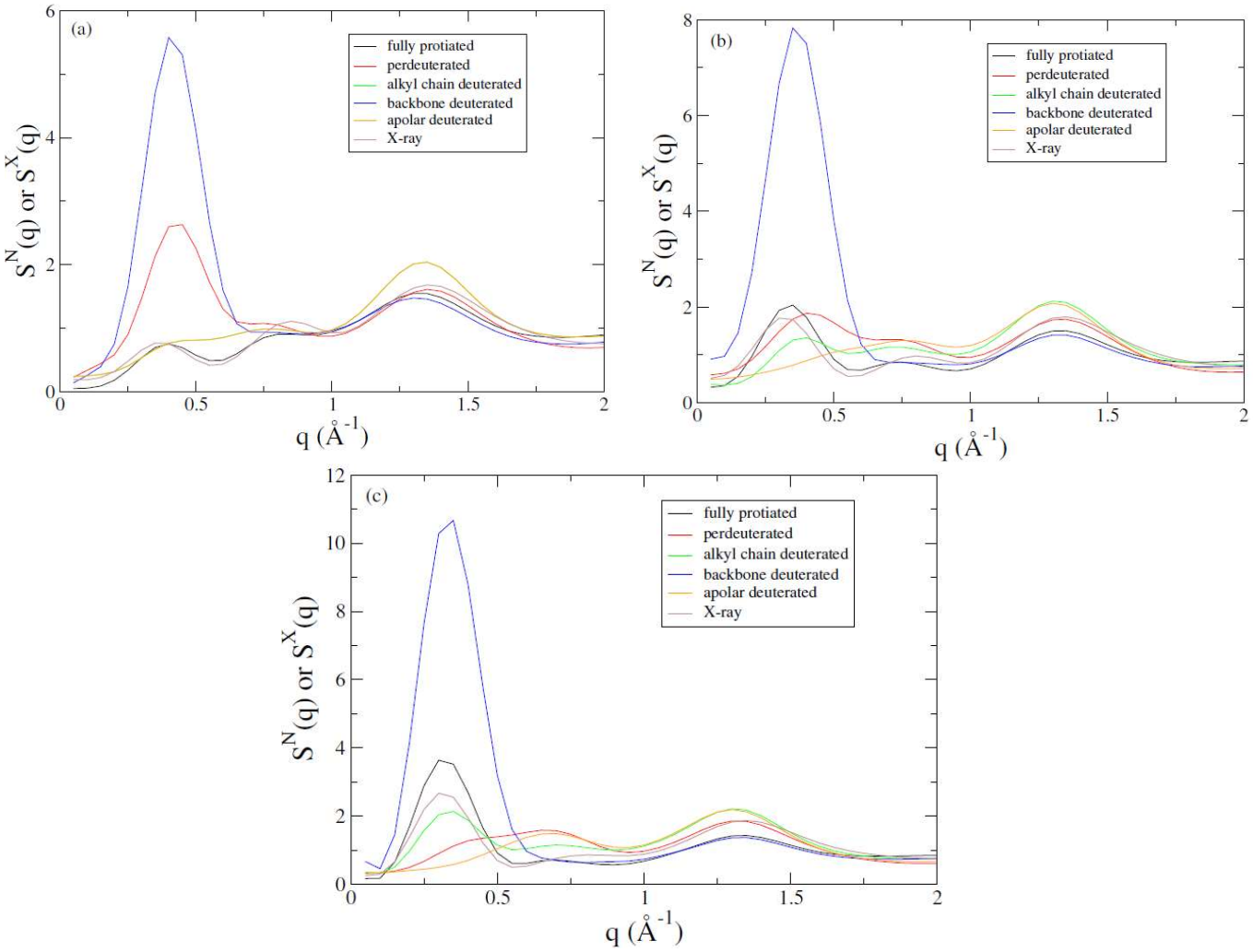

Figure 2. Simulated total neutron and X-ray structure factors of: (a) poly(C_3VIm Tf_2N), (b) poly(C_5VIm Tf_2N), and (c) poly(C_7VIm Tf_2N).

Several group contributions can be approximated using a common factor analysis of the neutron scattering data. Figure 3 presents a few constructive examples of such a manipulation. Subtraction of the scattering of a fully protiated sample from that of the alkyl chain deuterated or from that of the backbone deuterated represents the alkyl chain contribution or backbone contribution to the total scattering, respectively. The negative scattering length of the hydrogen atoms annihilates that of the bonded alkyl carbons and makes the entire alkyl chain almost invisible for neutron particles in the fully protiated sample when compared to the deuterated alkyl chain sample. The most pronounced feature is that the backbone correlation contributes significantly to the low-q peak, which substantiates the phenomenological assignment of the low-q peak as the

backbone-to-backbone peak by Winey and co-workers, whereas the alkyl chain contribution is a relatively weak antipeak. Both correlations shift to lower q and intensify with increasing alkyl chain length. The other two sets of difference scattering spectra are from the scattering of a perdeuterated sample minus that of an alkyl chain deuterated and the scattering of a perdeuterated sample minus that of an apolar (including both backbones and alkyl chains) deuterated, which approximate the contributions to the total scattering from the correlations of the cationic imidazolium ring plus backbone and imidazolium ring only, respectively. The contribution of the backbone plus imidazolium ring weakens, becoming negligible around C5 and C6, and then turns more negative with increasing n. The weaker contribution of the imidazolium ring with increasing n is also observed. The most dominant anion contribution to the low-q peak as demonstrated in our recent work is impossible to be identified without exploiting other isotopic substitution options (for instance, sulfur labeling 32S/33S in the Tf2N anion). This difference scattering analysis provides a complementary experimental alternative to the detailed decomposition of the total structure factor afforded in molecular simulations or EPSR modeling.

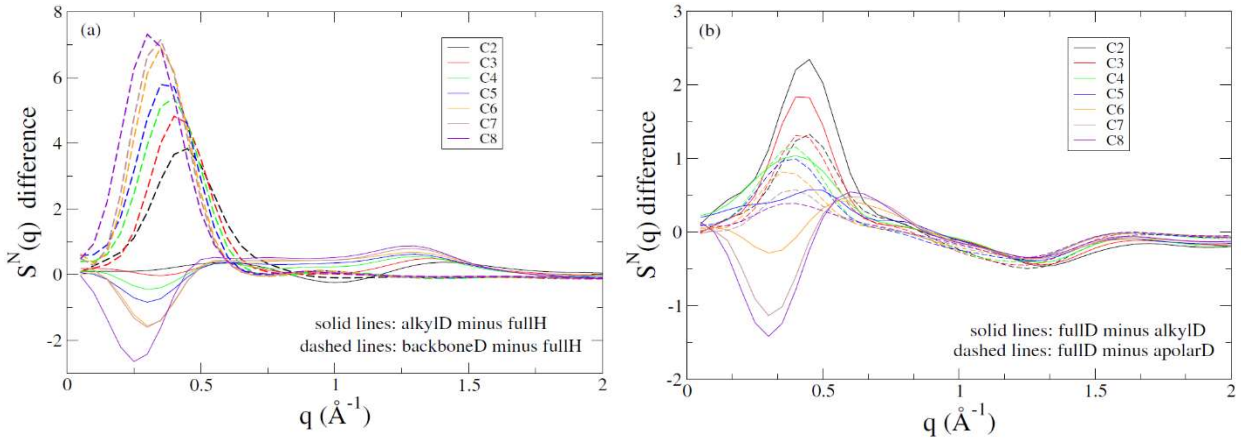

Figure 3. (a) Total neutron scattering differences of poly(C_nVim Tf_2N) showing the alkyl chain deuterated data minus fully protiated and the backbone deuterated minus fully protiated; (b) the perdeuterated minus alkyl chain deuterated and the perdeuterated minus apolar (including both backbones and alkyl chains) deuterated.

The scattering profiles in Figure 4 demonstrate that variation of the alkyl pendant length has an important influence on backbone-to-backbone spacing while variation in counter ion size appears to be most strongly reflected in pendant-to-pendant correlation lengths. As n increases from ethyl to hexyl, q_b shifts from 4.75 to 3.43 nm^{-1}. For the same series of polyILs, the side group correlation length remains constant at 0.46 nm, and the polar group correlation length ($d_i \approx 0.76$

nm) increases slightly with n. Our atomistic simulations indicate a progressive change in the nanoscale organization with increasing alkyl chain length. Structural analysis from the MD simulations yields correlation lengths in quantitative agreement with the experimental X-ray data (Figure 4a). Representative configuration snapshots reveal a tortuous polar network and progressive growth of nonpolar domains with increasing alkyl chain length. With increasing alkyl pendant length, discrete apolar islands first form within the continuous polar network and then grow beyond the percolation threshold, finally intertwining with the polar domains into a bicontinuous nanostructure (see Figure 5). These complex 3D networks are especially important in the context of ionic conductivity, as the actual pathways for the mobile ions are governed by geometric constraint. The apolar islands, which grow with increasing backbone-to-backbone correlation lengths, can be viewed as obstacles in the anion diffusion pathways resulting in reduction of the ionic conductivities. Similar transition to percolated structures with increasing volume fraction of polar groups was also observed in computational studies (coarse-grained and fully atomistic molecular dynamics) of ionomers by Frischknecht and co-workers.[4–6]

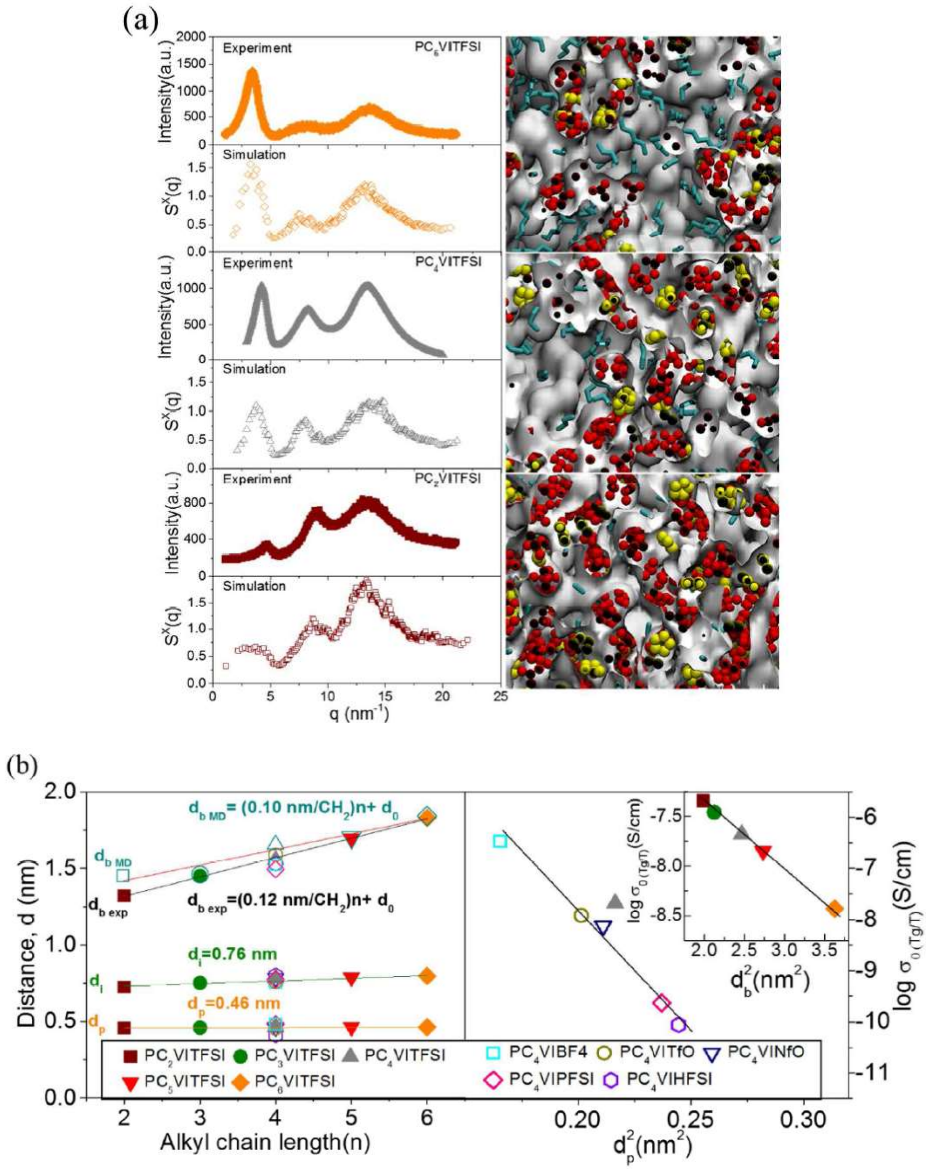

Figure 4. (a) Simulated X-ray scattering profiles of Poly ($C_nVIm\ Tf_2N$) (n = 2, 4, and 6) as functions of alkyl side chain length compared with experimental results. 3D tortuous contour surface (white colored) marks the ion transport channels (including all polar parts). Space-filling spheres in orthographic viewpoint are color coded: anions (red), and cationic imidazolium rings (yellow). Alkyl tails are represented by cyan segmented lines. All H atoms are omitted for clarity. Increasing apolar island size poses more constrictions to the inter-connectivity of percolating polar network, thereby lowering the ionic conductivity. (b) Left: Correlation lengths d_b, d_p and d_i Poly ($C_nVIm\ X$), where: $X^- = BF_4^-$, TfO^-, NfO^-, Tf_2N^-, $PFSI^-$ and $HFSI^-$; Right: dc conductivity at specified T_g/T as a function of pendant-to-pendant correlation distances. Inset: backbone-to-backbone correlation distances for the polyILs with Tf_2N^-. The error bars are comparable to the size of the symbols, if not specified otherwise. An exponential correlation is found between dc conductivity and d_b^2 for varying alkyl chain lengths and d_p^2 for the series of anions.

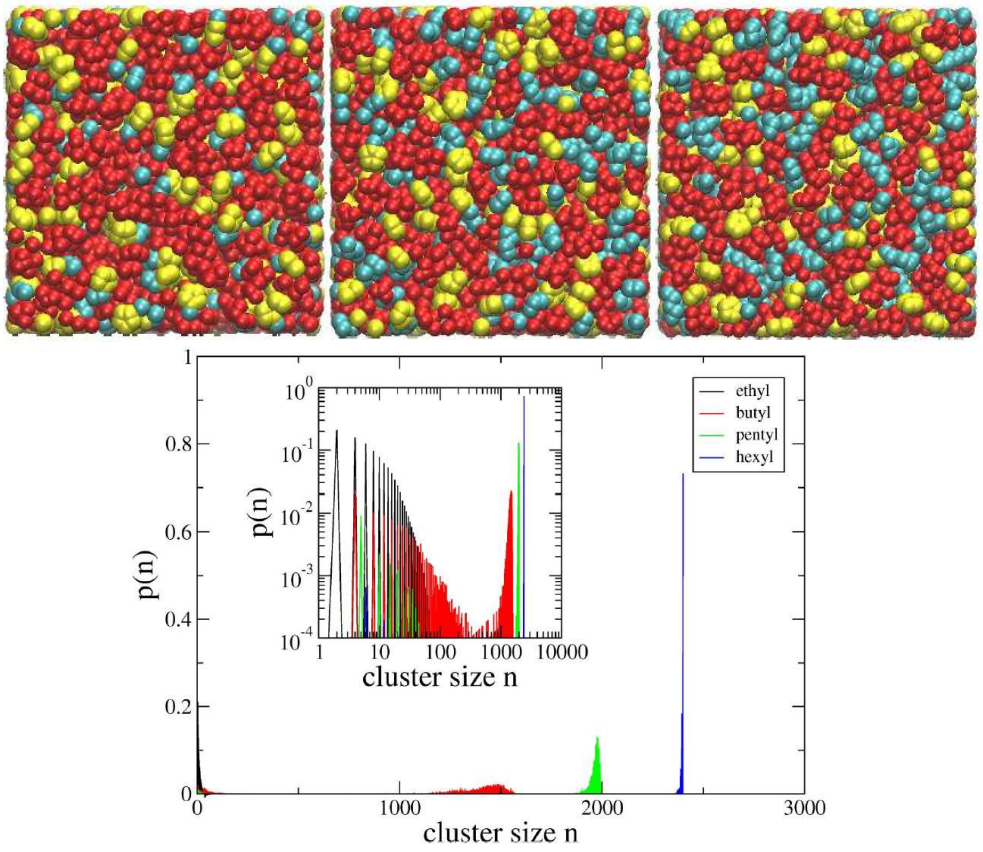

Figure 5. Upper: Ubiquitous polar network and ever-growing non-polar domain. (upper panel) Representative snapshots of Poly (C_nVIm Tf_2N) (n = 2, 4, and 6 from left to right). All H atoms have been omitted for clarity. Snapshots are shown with three-color space-filling models to reflect the presence of a polar network (red + yellow spheres). Color codes: anions (red), cationic imidazolium rings (yellow), and cationic alkyl chains (cyan). The simulation box length is 56.03, 58.52, and 60.80 Å for ethyl, butyl and hexyl polyILs, respectively. Lower: Cluster size distribution of non-polar domains of Poly (C_nVIm Tf_2N). Inset: the plot on a log-log scale.

Utilizing the broadband dielectric spectroscopy (BDS), the poly(2-trimethylammoniumethyl)-methacrylate [poly(C_nMTMA)] system yields a mean jump length of only 6 Å, which increases to 7.3 Å when the alkyl chain length increases to hexyl as seen in the inset in **Figure 6**. These values are much longer than mean ion jump lengths found for low molecular weight ILs and the two should not be regarded as identical physical quantities. To check the validity of the calculated lengths, wide-angle x-ray scattering (WAXS) measurements, and corresponding atomistic molecular dynamics simulations were compared in **Figure 6**. Based on previous data for poly(methyl methacrylate) and imidazolium based polyILs, the peaks were found to correspond to the pendant group correlation distance, q_p, the ion-to-ion correlation lengths, qi, and the backbone-

to-backbone spacing, q_b. PolyILs with butyl and hexyl pendant groups show signatures of long-range order corresponding to q_b. However, this peak is not observed in methyl and ethyl samples.

This is not because there is an absence of order in the backbone packing of these short side chain samples, but rather a result of poor contrast to observe this packing in the X-ray scattering experiments. This picture is verified by MD simulations that show the neutron scattering patterns of deuterated analogues which reveal the existence of peaks corresponding to backbone-tobackbone correlation distances in the short chain ammonium systems as well. **Figure 7** displays this neutron scattering simulation data for deuterated and per deuterated ammonium-based polyILs. In the neutron scattering simulations, a peak corresponding to the backbone-to-backbone distances is clearly visible for all samples studied. Similar simulations have been previously performed for a series of imidazolium-based samples and compared to measured neutron scattering data. Neutron simulations also reveal an interesting configuration when comparing the length of the side chain of the polymer to the backbone-to-backbone distances. For methyl and ethyl ammonium polymerized ionic liquids, the projected side chain length is less than half the distance between neighboring backbones, indicating no interaction between side chains of neighboring polymers (inset **Figure 7**b). For polyILs with butyl and hexyl pendant groups however, the projected side chain distance exceeds half of the backbone-to-backbone distance, suggesting the formation of inter-polymer interaction of side chains. We conjecture that this is due to formation of non-polar regions resulting from aggregation of alkyl chains of neighboring pendant groups that can have a hindering effect on anion mobility. The WAXS and neutron scattering spectra of chain-deuterated and perdeuterated samples from the molecular dynamics simulations are able to reproduce the pendant group, ion-to-ion, and the backbone-to-backbone correlation distances. For methyl and ethyl systems, the backbone-to-backbone spacing is 15 Å and 15.3 Å, while the projected length of the side chain is only 6.2 Å and 6.8 Å, respectively. This indicates minimal interaction between pendant groups of neighboring chains. However, for the pendant group length of the butyl and hexyl systems, the length of the projected sidechain, 8 Å and 11 Å, meets or exceeds the length of half of the backbone-to-backbone spacing, which is only 16 Å and 17 Å, respectively. Sidechains of neighboring polymers of the longer alkyl chain polyILs are therefore able to interact and form nonpolar regions between neighboring chains. This change in local ordering can hinder the path of diffusing ions, resulting in higher activation energies associated with ion diffusion, and hence, decreased ionic conductivity.

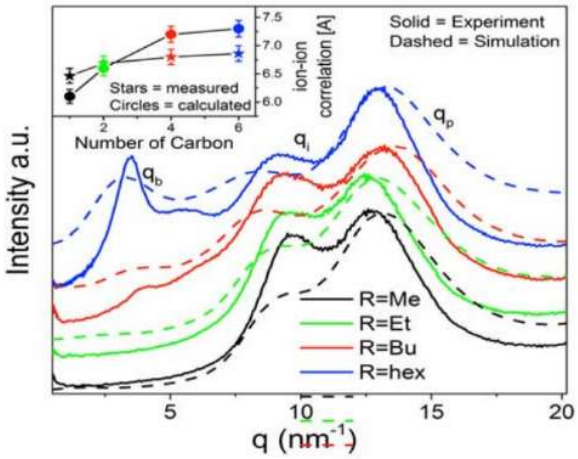

Figure 6. Experimental and simulated data of wide angle X-ray scattering (WAXS) for ammonium based polyIL with varying alkyl chain lengths, showing backbone-to-backbone correlation distances, q_b, ion-to-ion correlation distance, q_i, and pendant-to-pendant group correlation lengths, q_p. The inset shows mean characteristic ion diffusion distances calculated from BDS data and ion-to-ion correlation distances measured by WAXS.

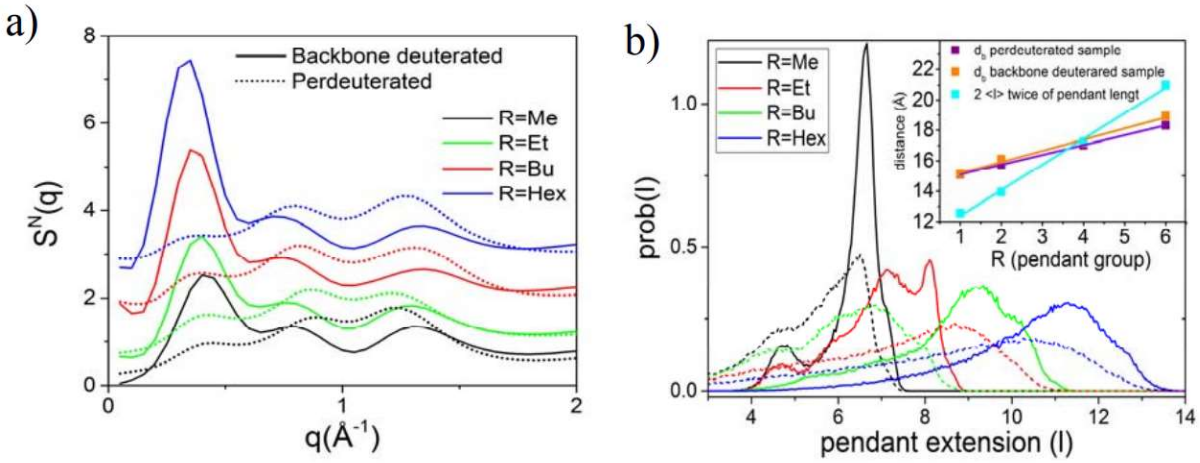

Figure 7. Neutron scattering simulation of deuterated and perdeuterated ammonium based polymerized ionic liquids with alkyl chain length, R, ranging from methyl to hexyl shown in a) for samples with deuterated backbone and perdeuterated side chains. The probability associated with the distance between backbone to the end of pendant group are shown in b) for extended and projected distances in solid and dotted lines, respectively. The distances obtained from a) and b) are shown in the inset of b) as functions of alkyl chain length for the series of polyILs.

The dynamics of ion hopping was firstly investigated from the hopping events defined as the formation and breaking of anion – cation association. An anion and a cation were considered as associated when the two are closer than the first coordination shell, i.e., closer than the local

minimum in the anion-cation radial distribution function (not shown here). Four hopping types were defined in **Figure 8** as type 1: intrachain, type 2: interchain, type 3: involving non-associating free anions and type 4: ions remaining intact. These hopping types are based on the formation and breaking of anion – cation association. Anion hopping was then categorized by comparing its associating cations at t and t+Δt. At either time, if the anion did not associate with any cation, then it was type 3. For an anion associated with cations at t and t+Δt, if the cations belonged to the same set of chains, the hopping was categorized into type 1, otherwise, it was type 2. If the anion had the same associated cations before and after, it was defined as type 4. The sampling time, Δt, was set to 10ps in these simulations. **Figure 9** compares the probabilities of the four hopping types for different anions. There are considerable numbers of intact anions in all the systems, which are denoted as type 4. Different sampling time has been tested that the shorter sampling time results in more intact anions as expected,[7] and the sampling time 10 ps is considered reasonable according to Mogurampelly et. al.[8] Intrachain hopping is 1.5 to 2 times of interchain hopping. Free anions without any association are rare to find. Increasing the temperature promotes interchain hopping obviously than interchain hopping for the polyatomic anions. The probabilities are not sensitive to the different charge models of Tf_2N.

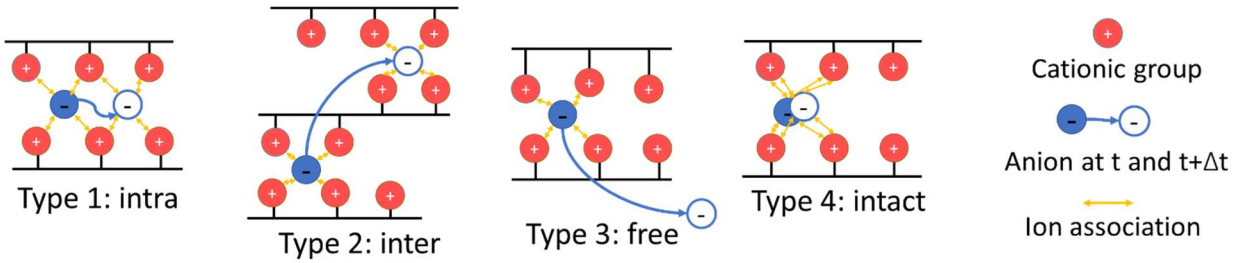

Figure 8. Definition of four types of hopping: (1) intramolecular (2) intermolecular (3) free (4) intact. The solid cyan circles and hollow cyan circles represent the position of anion at t and t+Δt, respectively, where Δt is the time resolution. Red circles pointed by the arrows are the associating cations.

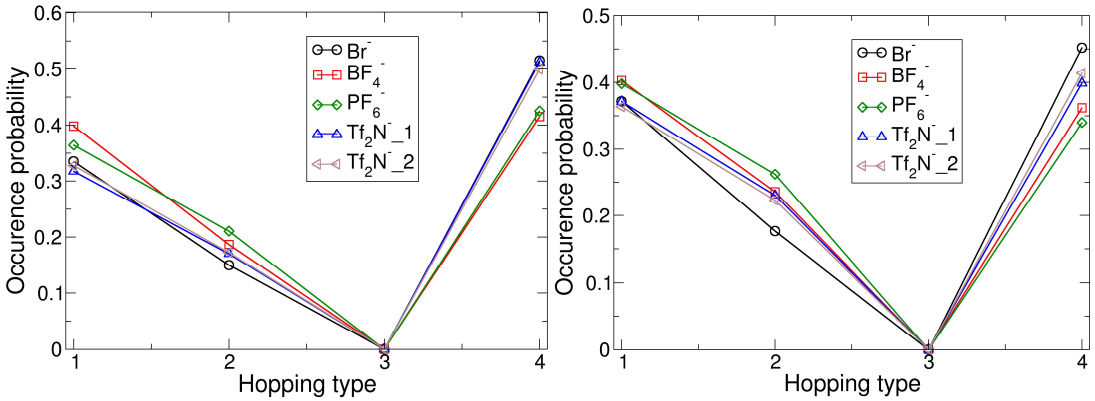

Figure 9. Comparison the occurrence probabilities of the four hopping types: left: 460K; and right: 550K. There are considerable intact anions in each system. Higher temperature resulted in the more increase of interchain hopping of polyatomic anion.

The diffusivity is calculated by the Einstein relation from the mean square displacement. **Figure 10** demonstrates the temperature effect on the diffusivity for different anions. Bromide has significantly lower diffusivity than the other anions. Generally, it is observed that the diffusivity shows the order of Tf_2N^- > BF_4^- >PF_6^- >Br^-. Tf_2N^-_1 shows some deviations from Tf_2N^-_2, especially at 460 and 600 K; the diffusivity of Tf_2N^-_1 is obviously lower than that of Tf_2N^-_2. Although it is of the same magnitude as the other polyatomic anions, it indicates the importance of careful calculation of the partial charges for the anions with multiple conformations.

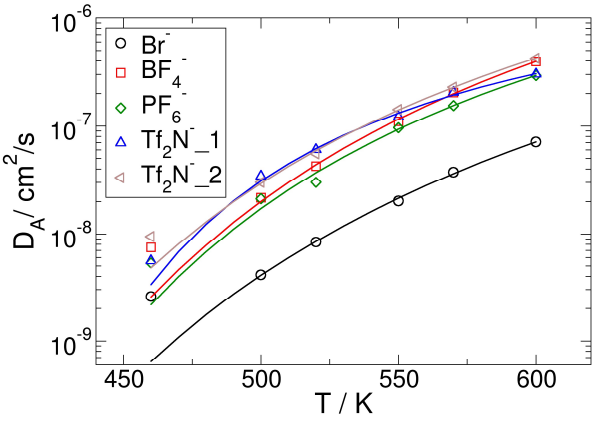

Figure 10. Diffusivities for the various anions computed with the Einstein relation from mean square displacements. Br^- exhibits a significantly lower diffusivity over the entire temperature range. Solid lines are the Vogel-Fulcher-Tammann (VFT) fitting. There is a discrepancy from the VFT equation at the lowest temperature.

To further investigate the relation between ion hopping and diffusivity, self-intermediate scattering function, $F_s(q,t)$, intermittent time correlation function, C(t), and continuous time correlation function, S(t), were calculated. The self-intermediate scattering function only represents the motion of the anions regardless of the cation – anion association, which is calculated by $F_s(q,t) = \langle \exp(i\mathbf{q} \cdot [\mathbf{r_i}(t) - \mathbf{r_i}(0)]) \rangle$, where $\mathbf{q}$ is the reciprocal wave vector and $q = |\mathbf{q}|$. The wave length $q^* = 0.76$ Å^{-1} is chosen for $F_s(q^*,t)$, which corresponds to the first peak of Anion-anion radial distribution function in real space.[9] The intermittent time correlation function, C(t), and a continuous time correlation function, S(t), are defined as $C(t) = \frac{\langle h(t)h(0) \rangle}{\langle h \rangle}$ and $S(t) = \frac{\langle H(t)h(0) \rangle}{\langle h \rangle}$, where h(t) is assigned to unity if an ion association is present at t = 0 and remains intact at time t, and H(t) has a value of unity if the ion association exists at t = 0 remains intact continuously up to time t. The two correlation functions denote the ion hopping events. The decay of C(t) can be regarded as the dissociation of the anion and cation without the recovering, while S(t) decays once the first-time dissociation takes place no matter the reassociation. The structural relaxation time, τ_c, and the average lifetime of ion-association, τ_s, are calculated by fitting C(t) and S(t) to a stretched exponential function and analytically integrated. The definition of the relaxation time is as follows:

$$F_s(q,t) \; or \; C(t) \; or \; S(t) = a_0 \exp[-\left(\frac{t}{a_1}\right)^{a_2}]$$

where a_0, a_1, a_2 are the fitting parameters, and the relaxation time τ_c and τ_s are calculated by

$$\tau_q \; or \; \tau_c \; or \; \tau_s = a_0 a_1 \Gamma(1 + \frac{1}{a_2})$$

where Γ is the gamma function.

Figure 11 plots the mean square displacement for an exemplar system poly(C_2VIm Tf_2N^-) and the diffusivity as functions of relaxation times. The mean square displacement shows the plateau, suggesting the cage effect of ion diffusion. Power law fitting $D \sim \tau^{-\lambda}$ were carried out for all the relaxation times. The fitted curves reveal that λ is approximately equal to 1 for τ_c but distinct from unity for τ_q or τ_s. The linear correlation of the diffusivity and $1/\tau_c$ seem to be in contradiction to the pioneering work of Ganesan et. al.,[8] where they demonstrated the relation of $D \sim \tau_s^{-1}$. However, this issue of $D \sim \tau^{-\lambda}$ is rather complicated. Subsequent work by Ganesan and coauthors also observed $D \sim \tau_s^{-1}$, or $D \sim \tau_c^{-1}$, or both the $D \sim \tau_s^{-1}$ and $D \sim \tau_c^{-1}$ for various polyILs with different cations.[10–13] The Bollinger et. al. also determined that $D \sim \tau_s^{-1}$ in a coarse-grained simulation

of ionic polymers.[6] **Figure 12** plots the $D \sim \tau_c^{-\lambda}$ and $D \sim \tau_s^{-\lambda}$ for different counterions. Although both graphs showed nearly $D \sim \tau^{-1}$ when fitting all the data points to the power law, the points are located closer to the $D \sim \tau_c^{-1}$ but more scattered from $D \sim \tau_s^{-1}$. These observations imply that the diffusion is correlated to the dissociation of the ion pair followed by the eventual departure from the 'cation cage'. We have also observed a plateau with the negligible displacement at 1 – 100 ps in the mean square displacement for Tf_2N^-, which indicates a non-diffusive regime at the time scale of ion pair dissociation (10 ps). Hence, the ion transport mechanism requires analyses of longer time scale, which is discussed below.

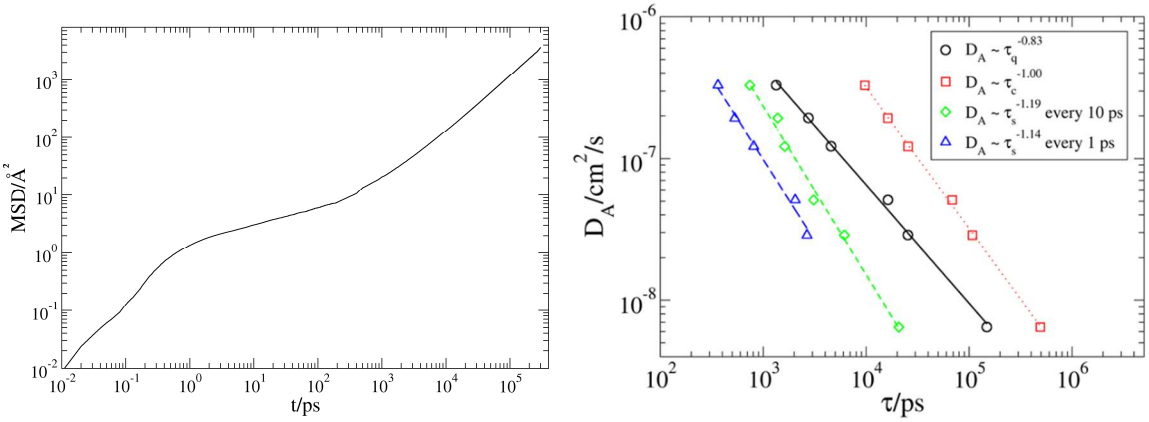

Figure 11. Left: Mean square displacement at 570K for poly(C_2VIm) Tf_2N^-_1; Right: Correlation between anion diffusivity and relaxation times. τ_s has two sampling times of every 1 ps and 10 ps, respectively, as a brief test.

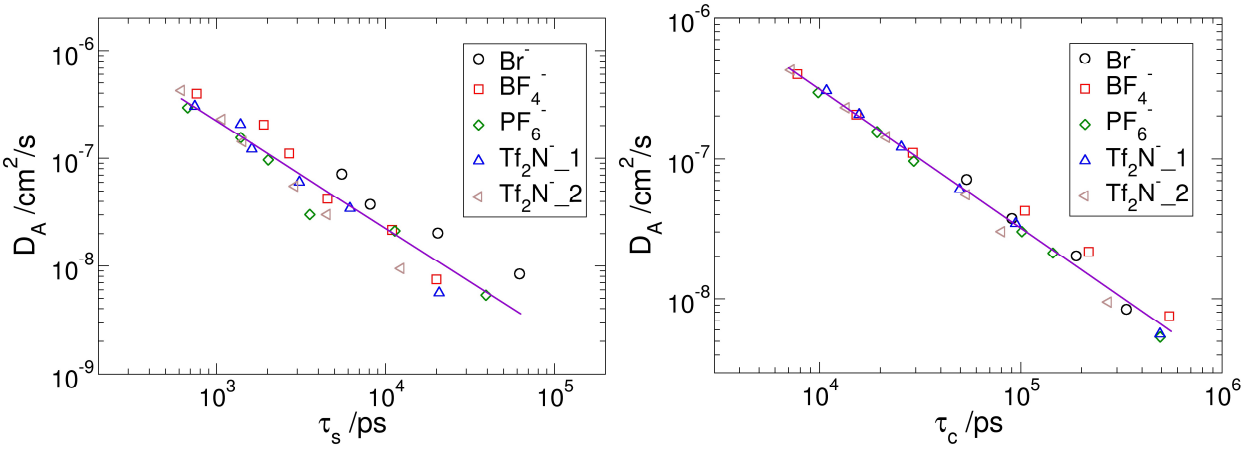

Figure 12. Left: $D_A \sim \tau_s$ plot; and right: is the $D_A \sim \tau_c$ plot for different counterions with $T \geq 460K$ and MSD > 100Å^2 in 300 ns. The power law shows that $D_A \sim \tau_s^{-0.9945}$ and $D_A \sim \tau_c^{-0.9867}$.

To further investigate the ion transport, the dynamical heterogeneity was characterized with the self-part of the van Hove function:

$$G_s(r,t) = \frac{1}{N}\sum_{i=1}^{N}\langle\delta(r - |\boldsymbol{r}_i(t) - \boldsymbol{r}_i(0)|)\rangle$$

where N is the total number of particles, $\boldsymbol{r}_i$ is the coordinates of the i^{th} particle, and δ is the Kronecker delta. $G_s(r,t)$ gives the distribution of the ion displacement. Ideally, the gaussian behavior of the self-part of the van Hove function is in the form:

$$G_{s,0}(r,t) = (\frac{3}{2}\langle r^2(t)\rangle)^{3/2}\exp(-\frac{3r^2}{2}\langle r^2(t)\rangle)$$

The degree of deviation from the ideal Gaussian behavior can be further quantified by the non-Gaussian parameter:

$$\alpha_2 = \frac{3\langle(\boldsymbol{r}(t) - \boldsymbol{r}(0))^4\rangle}{5\langle(\boldsymbol{r}(t) - \boldsymbol{r}(0))^2\rangle^2} - 1$$

which was calculated for the centers of mass of the anions in this research. The maximum of $\alpha_2(t)$ was extracted to quantify the dynamical heterogeneity, as shown in **Error! Reference source not found.**. Clearly, the maximum of α_2 (α_2^{max}) decreases with both the temperature and the volume of anion. It is speculated that the more flexible molecules enable the smoother motion of the anions, which can be the effect of plasticization. The two different charge models of Tf_2N^- does not significantly affect the dynamical heterogeneity. By extracting the characteristics of $\alpha_2(t)$, the time scale corresponding to the maximum of α_2 is recorded. In other words, t^* satisfies $\alpha_2(t^*) = \alpha_2^{max}$, which is the time scale when the non-gaussian behavior is the strongest. Temperature dependence of $G_s(r,t^*)$ is presented in Figure 14. Multiple peaks in $G_s(r,t^*)$ are characteristic of hopping motion of anions to preferentially quantized distances. In $G_s(r,t^*)$, there are the deep valleys between the two peaks for the smaller anions, but the two peaks are convoluted for Tf_2N^- to some extent. This is consistent with its lower α_2^{max}. Since $G_s(r,t^*)$ was calculated from the centers of mass of Tf_2N^-, the multiple conformation and non-spherical shape enable the local fluctuation and consequently, a smoother motion of anion. Although there is no significant valley for Tf_2N, the local minimum of $G_s(r,t^*)$ can be distinguished for all the simulated systems. This local minimum locates at r^* = 3.5, 3.9, 4.0, and 5.9 Å for Br^-, BF_4^-, PF_6^-, and Tf_2N^-, respectively. The r* value is used as the criterion to distinguish the mobile ions and the immobile ions. The former moved farther than r^* within a time interval of t^*, while the latter were staying inside the r^* range, most probably the rattling ones, as shown in **Figure 15**.

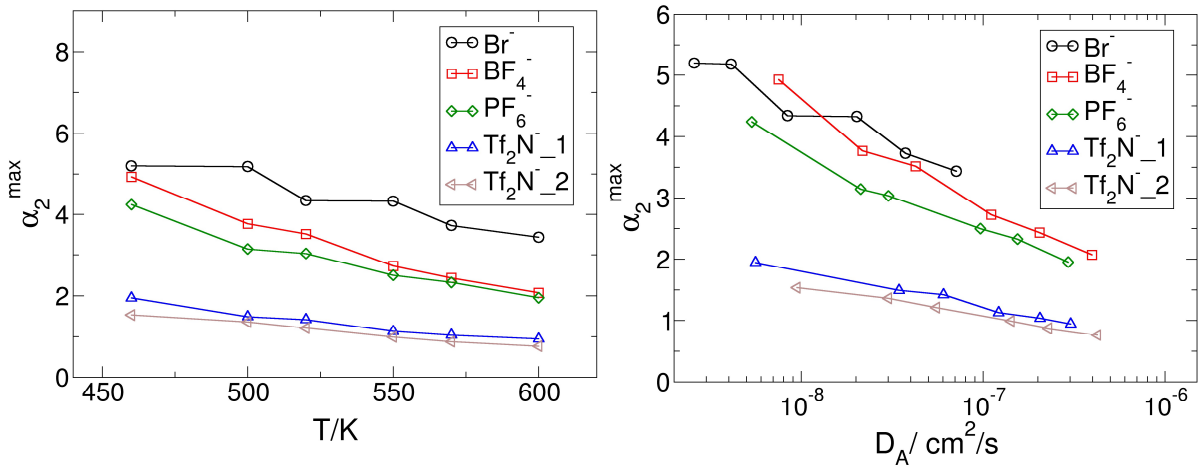

Figure 13. Properties of the non-Gaussian parameter α_2. Left: Maximum of α_2 as a function of temperature; and right: as a function of the diffusivity.

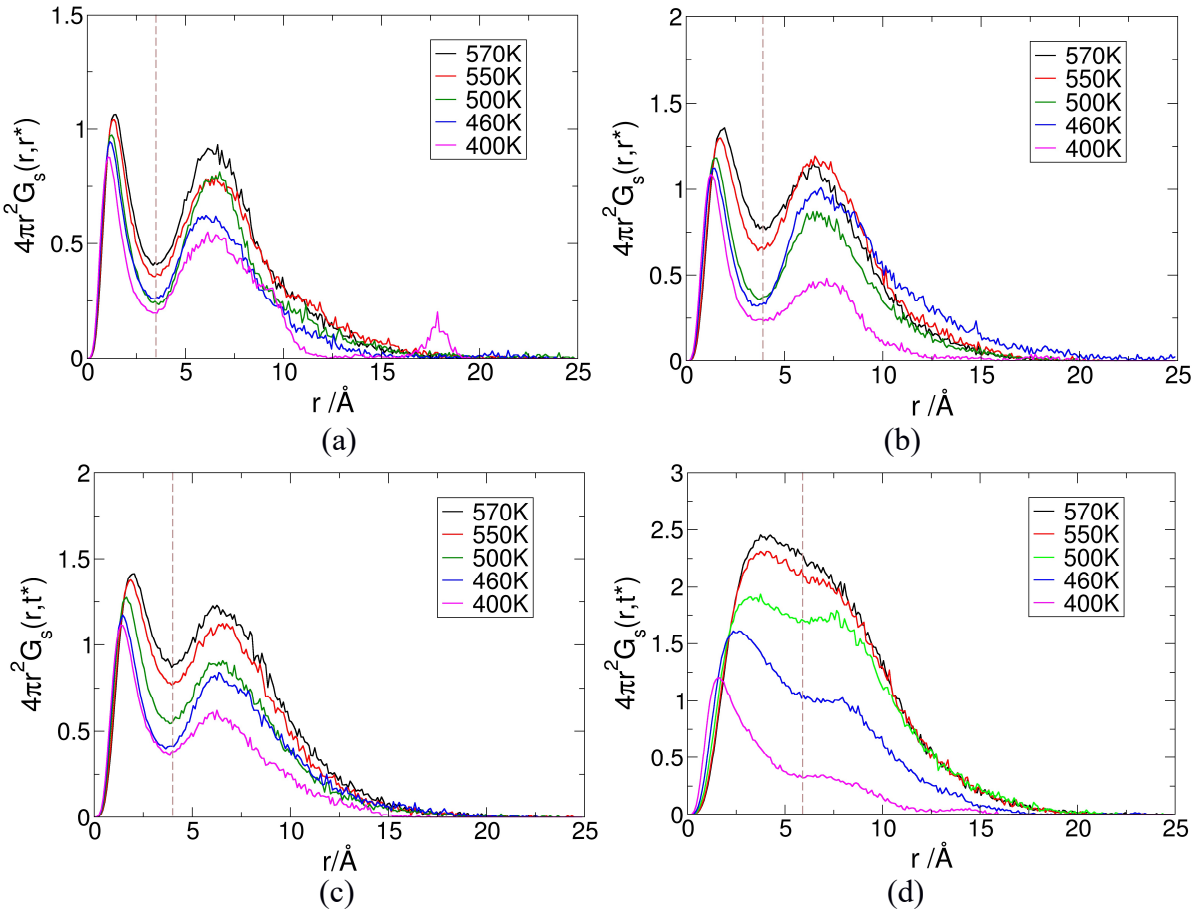

Figure 14. Self-part of the van Hove function at the time scales of t^*. (a) Br^-; (b) BF_4^-; (c) PF_6^-; (d) Tf_2N^-_1. The first local minimum defines the criterion of fast anion r^*. If the anion traveled farther than r^*, it was defined as fast mobile anion, otherwise, it was categorized as slow immobile anion. Note that Tf_2N^- has two convoluted peaks, while the other anions show significant valleys.

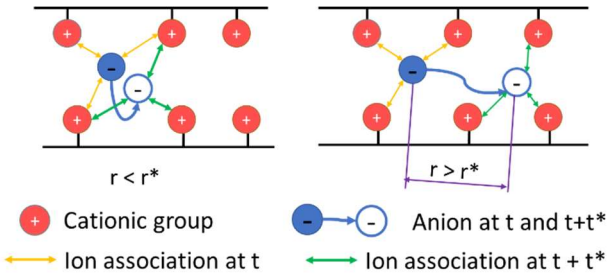

Figure 15. Hopping of only the ion pair dissociation (left) in comparison with the effective hopping (right) where the ion travels farther than the distance r* in time t*.

The percentage of mobile ions are about 10% to 15% at 600K, and 6% to 10% at 460K for the different anions. Generally, Br^- has the lowest percentage of mobile ions, which is consistent to exhibiting the lowest diffusivity. This work confirms the property of the small percentage of mobile anions in polyILs. It is worth noting that there are significantly fewer mobile ions than hopping ions in **Figure 9**, albeit the sampling time interval t* is much longer than Δt. As a result of this significant difference, the dissociation and association at short time scales, is not sufficient to explain the transport behavior. The anion experiences the effective hopping when it leaves the original coordination cage and travels farther than r* in t*, and the anion is mobile. In contrast, if the anion only breaks or forms association but does not travel the distance of r > r*, there may be continuous dissociation events, but these events will not lead to actual transport.

To further study the motions of the ions, the distinct part of the van Hove function, $G_d(r,t)$. is computed for all counterions. $G_d(r,t)$ is defined as:

$$G_d(r,t) = \frac{1}{N}\sum_{j\neq i}^{N}\langle\delta(r - |\mathbf{r_i}(t) - \mathbf{r_j}(0)|)\rangle.$$

Figure 16 plots the $G_d(r,t)/4\pi r^2\rho$ for Br^-, BF_4^-, PF_6^- and Tf_2N^-_2 at 550K, where ρ is the numerical density of the anion. More results for Tf_2N^-_1 and the temperature of 460K can be found in our publication.[3] The non-trivial peaks at r = 0 indicates correlated motion, where it is possible for an anion to occupy the position of another anion as a replacement. The much higher peak at r = 0 for Br^-, BF_4^- and PF_6^- indicates the precise replacement, while the lower peaks for Tf_2N^- is probably due to its flexibility as the center of mass of Tf_2N^- has more freedom to fluctuate. For Br^-, BF_4^- and PF_6^-, the peak at r = 0 immediately increases at t = 100 ps, while for Tf_2N^-it rises at t = 500 ps. Due to the limited sampling frequency and trajectory collection, it is hard to find the exact time when the correlated motion begins to appear. However, Tf_2N^-, the largest anion, clearly requires a longer time to exhibit correlated motion.

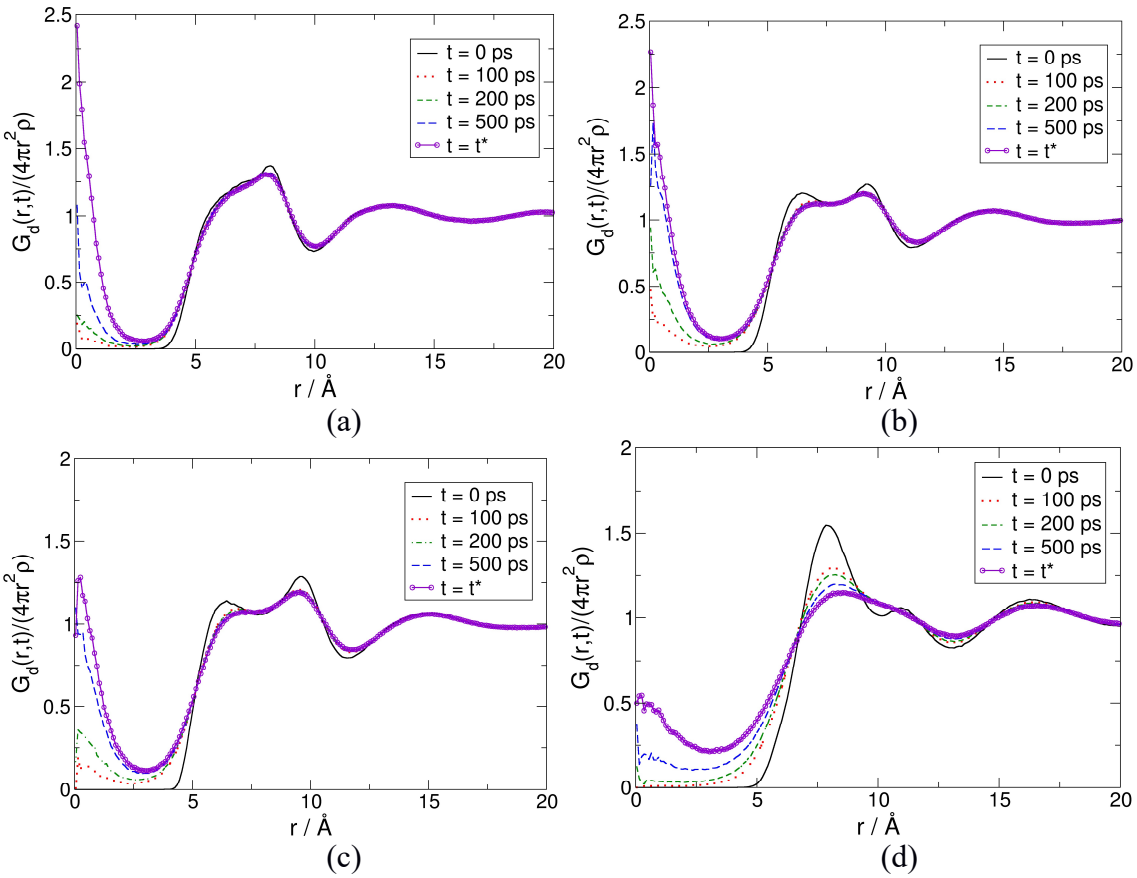

Figure 16. Distinct part of van Hove function at 550K with different sampling intervals: (a) Br^-; (b) BF_4^-; (c) PF_6^-; and (d) Tf_2N^-_2. Non-trivial peak at r=0 appears at shorter sampling time for Br^-, BF_4^- and PF_6^- than Tf_2N^-_2.

The stringlike cooperative motion has been reported in supercooled liquid and glass-forming Lennard-Jones liquid,[14,15] as well as ionic liquids.[16] Considering the correlated motion as mentioned above, this research have attempted to search for this phenomenon in polyILs. The i^{th} and j^{th} anions are in the same string if their centers of mass satisfy:

$$\min\left[\left|\boldsymbol{r}_i(t) - \boldsymbol{r}_j(0)\right|, \left|\boldsymbol{r}_j(t) - \boldsymbol{r}_i(0)\right|\right] < r_S$$

where $\boldsymbol{r}$ is the position of anion and r_S is the cutoff distance. The string connection between mobile anions were checked at t = 0 and t = t* by the equation above. The cutoff distance was set to 2.1 Å for bromide and 2.2 Å for the polyatomic anions, which were approximately the "hard core" radii. **Figure 17** is the snapshot of a string in poly(VIm Br) as an example, which provides the visual concept of string-like motion.

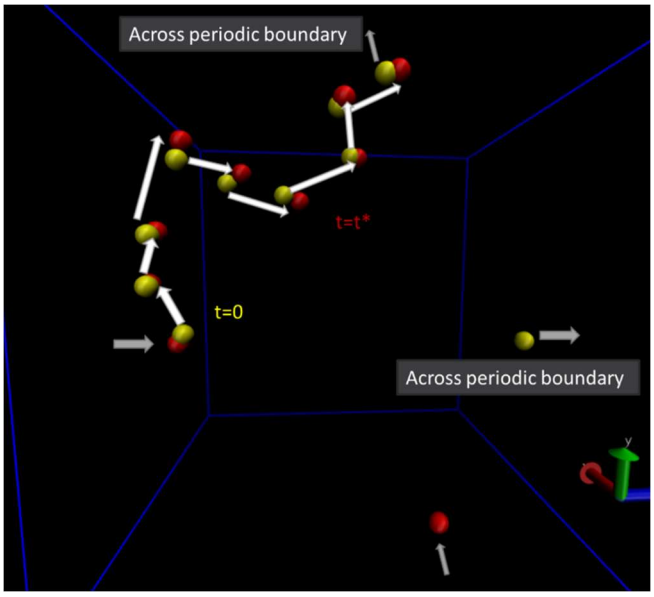

Figure 17. String-like motion of anions from the simulation of Br^-. The yellow beads are the anions at t = 0. The red beads are the anions at t = t^*. The white arrows show the hopping path. The blue lines are the edges of the simulation box.

To quantify the number of mobile anions or string length (n_s), the temperature dependence the string length distribution, P(n_s), is shown in **Figure 18**. The zero length is artificially defined as the immobile anions, and consequently, it shows that most anions are slow immobile ions. Recalling that t* is much longer than the sampling time of association/dissociation-based hopping. It can be anticipated that the cation – anion dissociation happens at a much shorter time scale than the actual ion hopping farther than a certain distance criterion. It is noticed that a considerable portion of mobile ions were hopping with n_s=1, i.e., not forming a string. Despite the relatively high percentage of n_s=1, longer strings are found, and thus the stringlike motions are confirmed. Longer strings are found to have smaller percentages. Comparing the four anions, the longest string decreases with the size of anion. For example, Tf_2N^- forms the longest string with n_s=8, but Br^- and BF_4^- have the longest strings approximately of n_s=15. In Figure 18(d), average string length is plotted for all the simulated systems. The average string length generally decreases with the temperature for T≥440K and the discrepancies at T<440K may be due to the very slow dynamics. Comparing the different anions, larger volume generally tends to have shorter average string lengths that Br^- and BF_4^- > PF_6^- >Tf_2N^-. The charge model of Tf_2N^- does not affect the average string length.

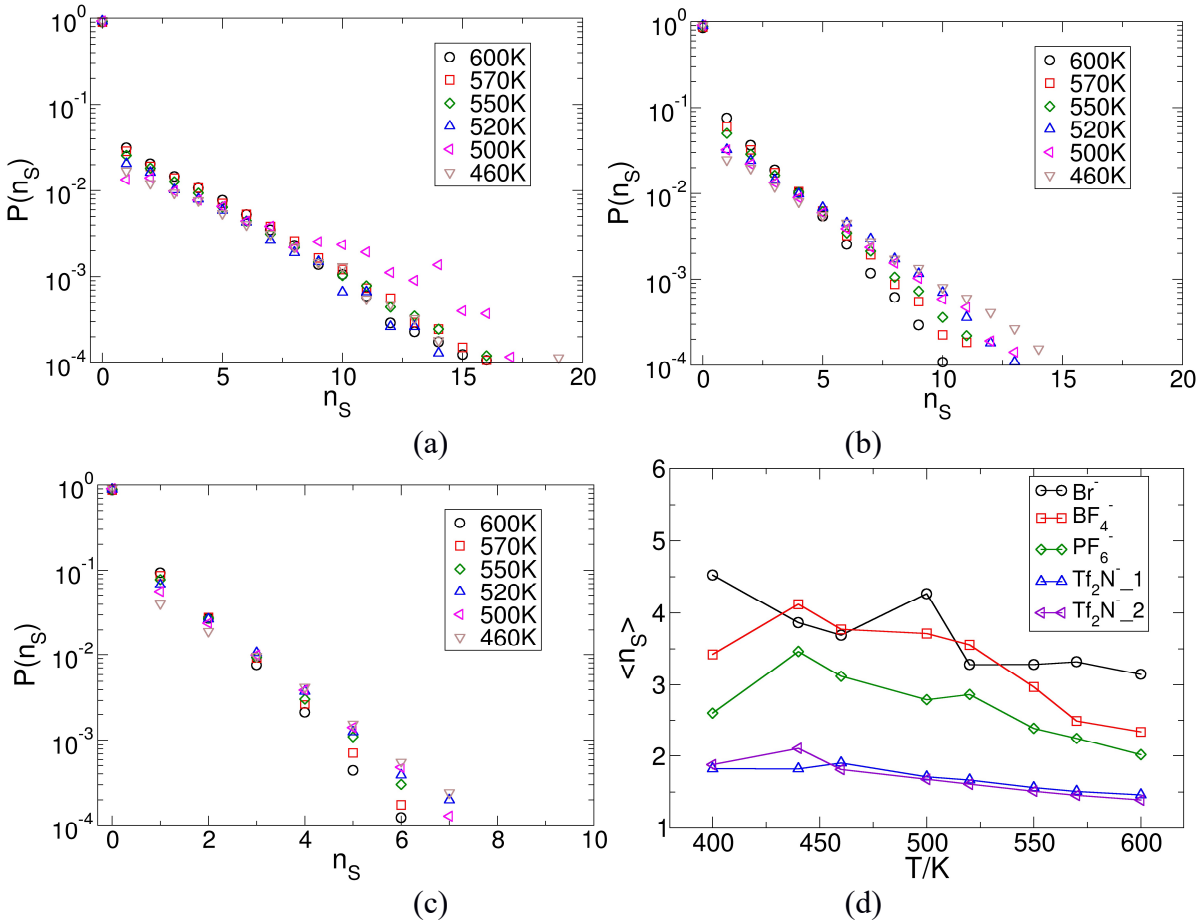

Figure 18. Length of string like motion. Length distribution: (a) Br^-; (b) PF_6^-; (c) Tf_2N^- (Tf_2N^-_2); (d) Average length of string like motion. Only the strings with the probability greater than 10^{-4} are considered. The string length generally decreases with the temperature for T≥440K, except Br^- at 500K. The discrepancies at T<440K may be due to the very slow dynamics.

The above analyses were then applied to the poly(C_nMTMA Tf_2N) systems. Poly(C_nMTMA) and poly(C_nVIm) have an important difference in the chemical structure. The former material possesses a longer linker connecting the cationic head group to the polymer backbone, while the latter has the imidazolium group grafted directly to the backbone. The existence of the long linker creates flexibility in the ammonium head groups and hence less constraint by the polymer backbone. **Error! Reference source not found. Figure 19** shows the distributions of the cation-backbone distance and the backbone-side chain angle for poly(C_2MTMA Tf_2N) and poly(C_2VIm Tf_2N) at 500K. It is clear that the longer linker significantly flattens both curves as expected, which indicates the less constrained head group in poly(C_nMTMA).

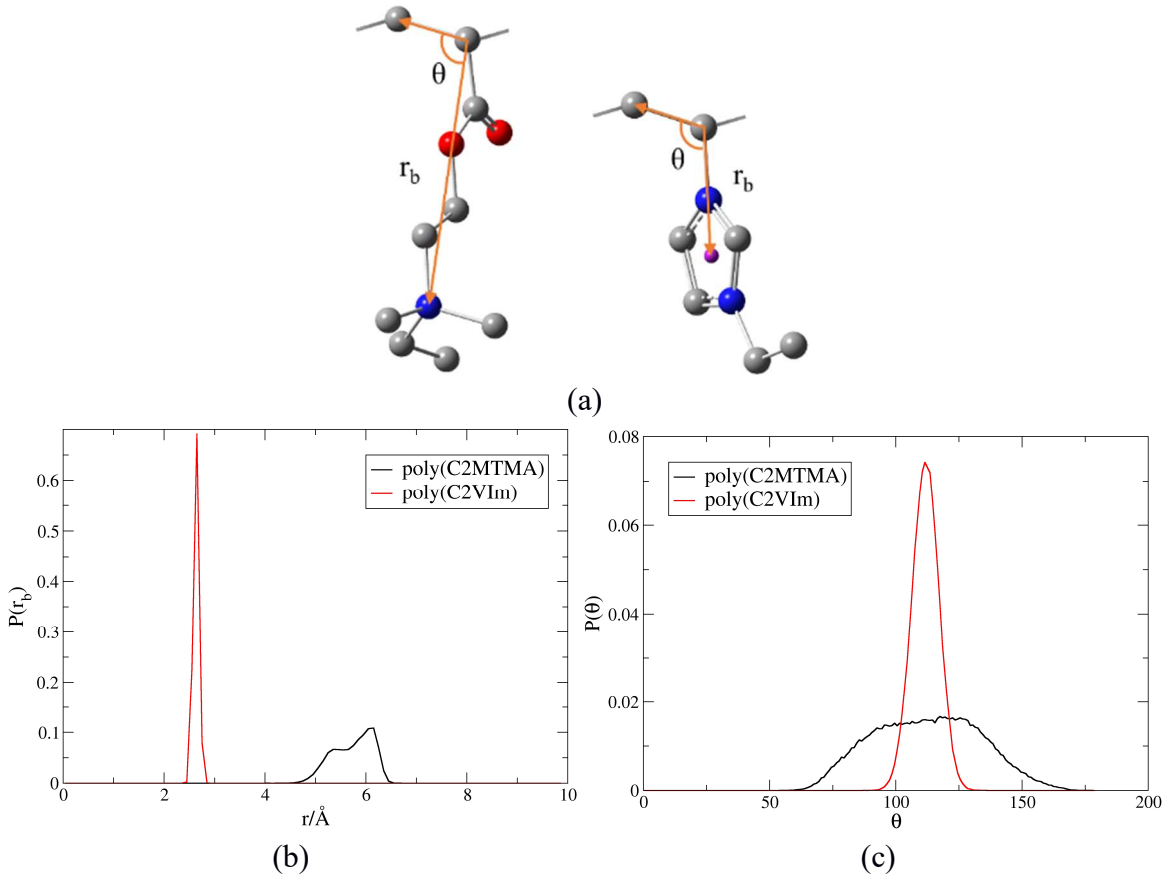

Figure 19. Measurements of backbone – cation distance and backbone – side chain angle at 500K. (a) The definitions of the distance and angle for the different polymerized cations. (b) Distribution of distance. (c) Distribution of angle. Poly(C_2MTMA) has uniform distributions of the backbone – cation distance and the backbone – side chain angle.

The probabilities of hopping types defined in **Figure 9** are demonstrated in **Figure 20** at low and high temperatures. There is no free anion with no associated cationic group (type 3) in the systems due to the strong electrostatic interaction. The side chain length affects the hopping events, which is denoted by the arrows. Intrachain hopping (type 1) increases from C1 to C2, and then it decreases with the side chain length. When the side chain has reached C4, it shows less type 1 hopping compared with the shortest side chain of C1. The interchain hopping (type 2) also shows the peak probability with the side chain length. It increases from C1 to C3 and then decreases from C3 to C6. Type 4 (intact) represents the percentage of the anions which are not involved in ion pair dissociation. It is found that C2 side chain has the lowest portion of rattling anions. Decreasing and increasing the side chain length from C2 lead to more type 4, which means the less sum of

type 1 and type 2. The longer side chains of C5 and C6 show the more type 4 than the shorter side chain lengths.

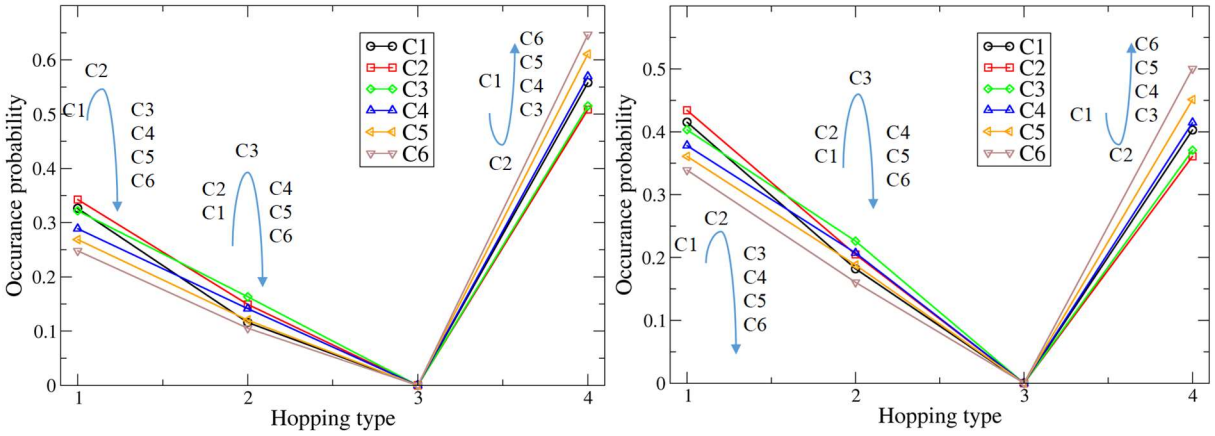

Figure 20. Four hopping types at different temperatures: left: 460K; and right: 550K. The resolution was set to 10 ps. The probability of each hopping type is affected by the side chain length.

Figure 21 provides the diffusivities calculated by the Einstein relation. The general conclusion can be drawn that the diffusivity increases with the alkyl tail length at the same temperature. Specifically, the shortest side chain C1 shows the much lower diffusivities compared with the other three materials, and the longer side chains of C4 and C5 have very close diffusivities for most simulated temperatures. The influence of side chain length reproduced the experimental results, thought the simulated temperatures are higher than experiment.[17] However, the simulated diffusivities are lower by magnitude from the experimental measurements, which can be due to the nonpolarizable force field.[12] The diffusivity of Tf_2N^- in poly(C_2MTMA) is much higher at the same temperature when compared with poly(C_2VIm), which can be attributed to the more flexible side chain in the molecular structure.

To examine the relation between the diffusivity and relaxation time, the average lifetime of ion association, τ_s, and the structural relaxation time, τ_c, were extracted. The sampling time of τ_s was set to 10 ps. **Figure 22** shows the diffusivity (D_A) as a function of the relaxation time for poly(C_nMTMA)Tf2N. Fitting the data to the power law yielded: $D_A \sim \tau_s^{-1.268}$ and $D_A \sim \tau_c^{-1.060}$. For all the materials, the exponent λ varies from 1.243 to 1.287 in $D_A \sim \tau_s^{-\lambda}$ for different alkyl tails, and 1.017 to 1.088 in $D_A \sim \tau_c^{-\lambda}$. The nearly unchanged exponents for each material demonstrate that the diffusivity is correlated to the structural relaxation, τ_c^{-1}, but not the ion association, τ_s^{-1}.

Recalling the regressions **Figure 12**, it varied from 0.836 to 1.297 in $D_A \sim \tau_s^{-\lambda}$ and 0.899 to 1.124 in $D_A \sim \tau_c^{-\lambda}$ for different anions when paired with poly(C_2VIm). Thus, it can be concluded that the exponent λ is affected by the chemistry of the anion (counterion), especially in $D_A \sim \tau_s^{-\lambda}$. Nevertheless, the linear correlation between the diffusivity and τ_c^{-1} for poly(C_nMTMA)Tf2N supports that the eventual dissociation of ion pair is the mechanism of ion transport in polyILs.

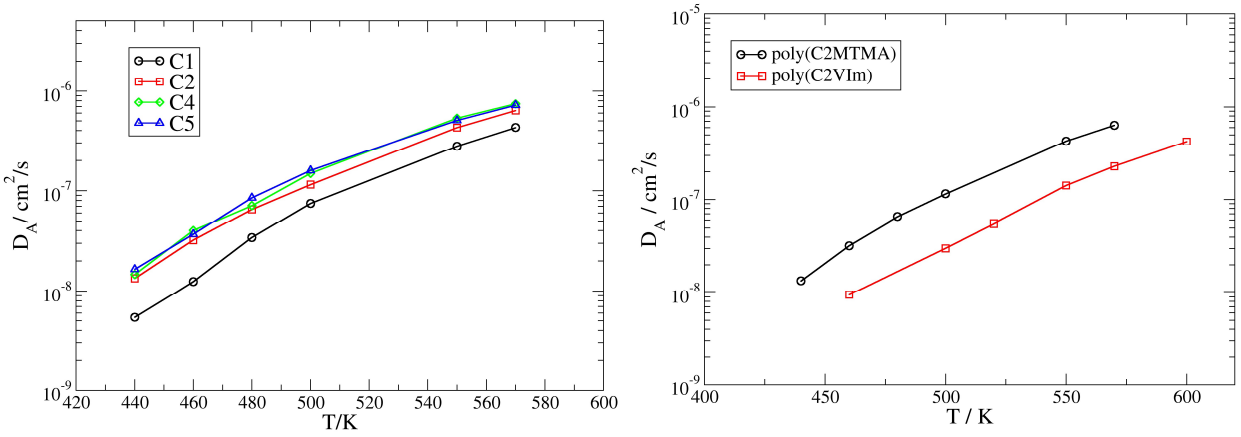

Figure 21. Left: Diffusivity (D_A) of Tf_2N^- in poly(C_nMTMA); and right: the comparison poly(C_2MTMA) with poly(C_2VIm).

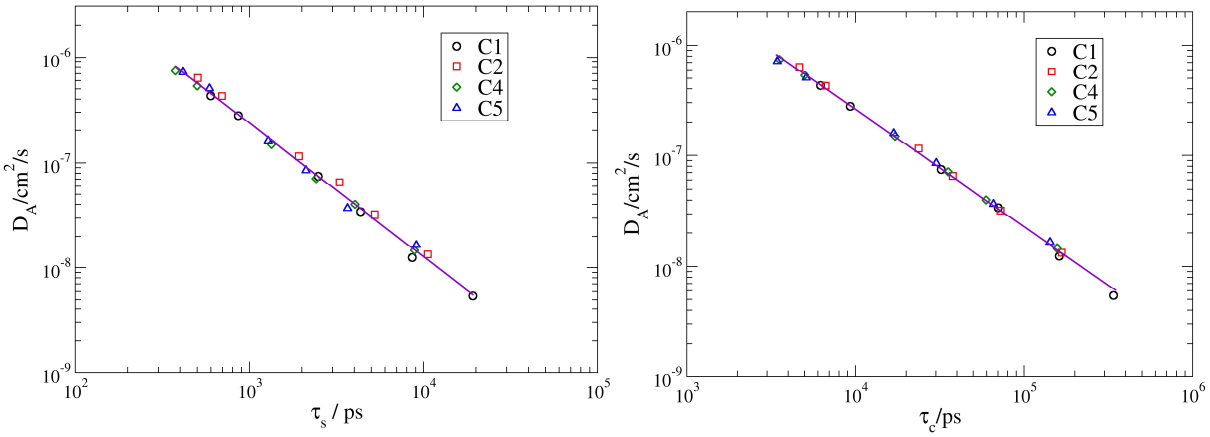

Figure 22. Relation between diffusivity of anion (D_A) and relaxation time for poly(C_nMTMA) Tf_2N. Left: D_A vs. τ_s; and right: D_A vs. τ_c. Only the data points with $T \geq 440K$ and MSD>100Å^2 in 300 ns are included for better statistics. The power law shows that $D_A \sim \tau_s^{-1.268}$ and $D_A \sim \tau_c^{-1.060}$.

For the dynamical heterogeneity, non-gaussian parameters (α_2) were calculated and the α_2^{max} was extracted, as shown in **Figure 23**. The shortest pendant tail C1 has the more developed heterogeneity that the maximal of α_2 is much higher. Poly(C_2MTMA) has the lower α_2^{max}

compared with poly(C_2VIm), which reflects the less heterogeneity in Poly(C_2MTMA). The longer linker can play an important role. The flexible linker enables some freedom of the head group, and thus the ion association cages are not strictly confined to the polymer chain. This local movement is thermodynamic and offsets the dynamical heterogeneity.

The self-part of van Hove function ($G_s(r,t^*)$) was investigated at the time scale t* satisfying $\alpha_2(t) = \alpha_2^{max}$. **Figure 24** shows the calculated $G_s(r,t^*)$ for poly(C_2MTMA) at 500K as an example in comparison with poly(C_2VIm). It is found that the $G_s(r,t^*)$ for poly(C_2MTMA) does not show the evidence of two separated peaks, which is very apart from the $G_s(r,t^*)$ for the poly(C_2VIm). This is consistent with the much lower α_2^{max}. The lack of distinguishable peaks implies the unconventional hopping, which could be the integration of anion hopping and the relatively free-moving polymerized cations. Thus, the distance of ion hopping, r*, was not able to be determined by the valley between the two peaks. There are other methods for r*, such as comparing the $G_s(r,t^*)$ with the gaussian behavior $G_{s,0}(r,t^*)$,[18] or fitting $G_s(r,t^*)$ to a superposition of two distinct mobility groups.[19] This work used the former method that r* is located at the intersection of $G_s(r,t^*)$ and $G_{s,0}(r,t^*)$, where $G_s(r^*,t^*) = G_{s,0}(r^*,t^*)$. For the consistency, $G_s(r,t^*)$ was reexamined with this new method for poly(C_2VIm) Tf_2N, and the obtained r* varies from 4.9 to 5.5 with the temperature from 460 to 570K, which is smaller than the criterion of 5.9 Å utilized in above. In the following paragraph, the analyses of poly(C_2VIm) Tf_2N were remade with the newly obtained r*.

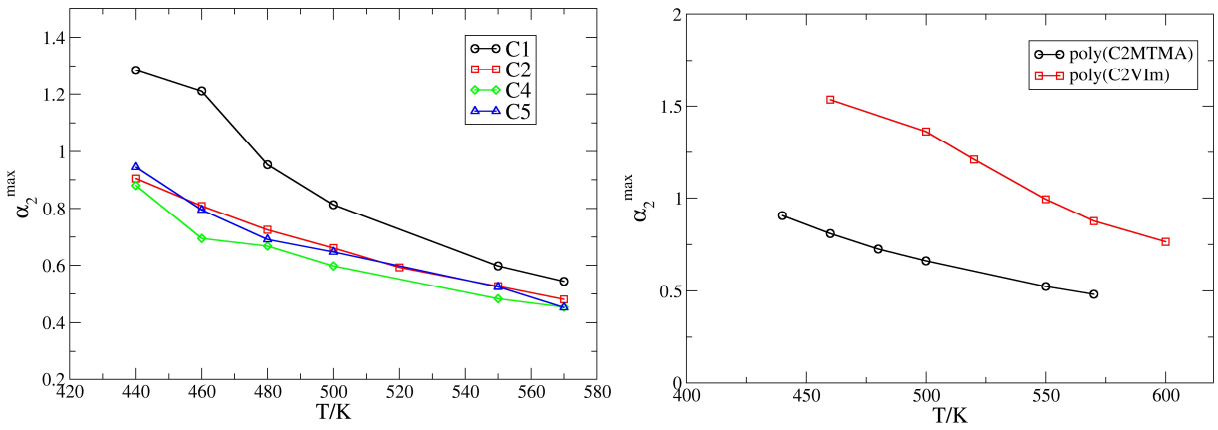

Figure 23. Left: Maximal of the non-Gaussian parameter (α_2); Right: comparison of poly(C_nMTMA) with poly(C_2VIm).

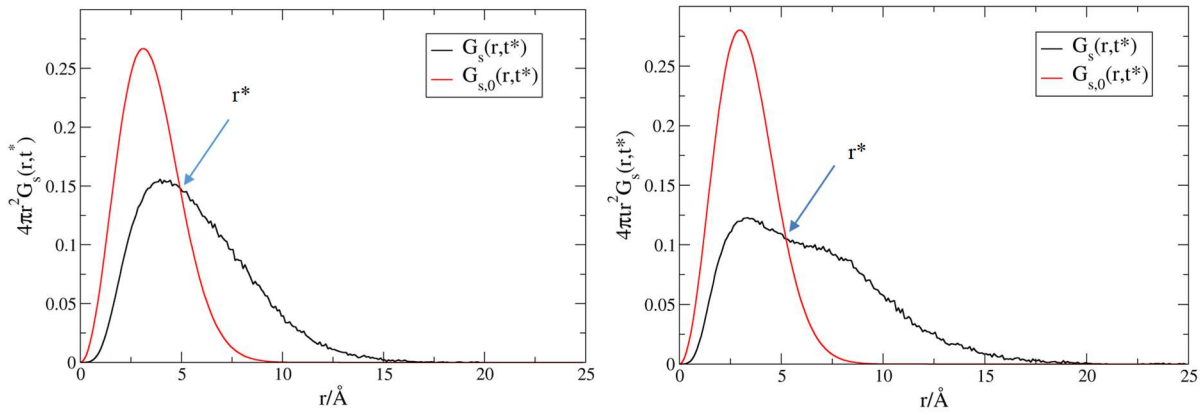

Figure 24. Self-part of the van Hove function [$G_s(r,t^*)$] of Tf_2N^-. Left: Poly(C_2MTMA); and right: poly(C_2MTMA) at 500K. $G_s(r,t^*)$ does not show distinguishable peaks, especially for Poly(C_2MTMA). $G_{s,0}(r,t^*)$ exhibits gaussian behavior. The length scale, r*, is defined as $G_s(r,t^*) = G_{s,0}(r,t^*)$.

The string-like motion of Tf_2N^- was studied by the same method as discussed above. The string length distributions are shown in **Figure 25**, which only include the strings with the probability larger than 10-4. The zero length represents the slow immobile ions. All the materials have most counterions as immobile ones, which make up about 80% of the total counterions. The probability of short string is much higher than long string. The longest string for each material decreases with temperature. For example, the string of 8 anions is found for C1 tail at 440K, but only the strings of 5 anions are found at 550K and 570K. For longer tails of C4 and C5, it is shortened by the increasing temperature that 5 anions and 4 anions are found in the longest strings at lower and higher temperatures, respectively. Longer pendant tail generally leads to less counterions in each string of the cooperative motion. The C1 material has the longest strings containing 5 – 8 anions at various temperatures, while C5 only has 4 – 5 anions. The average string length was calculated only for the string length equal to or greater than 1. It generally decreases with the temperature, but there are the exceptions especially for the lowest simulated temperatures for C1 tail. This smaller $\langle n_S \rangle$ can be due to the fewer fast mobile anions. The average string length shows the sequence of C1 > C2 > C4 ≈ C5, which is consistent with the diffusivity. **Figure 26** compares the poly(C_2MTMA) with the poly(C_2VIm). For poly(C_2VIm), string length analysis was performed using the newly updated criterion r* for fast mobile ions. The smaller r* resulted in slightly more mobile anions than **Figure 18**, i.e., fewer immobile anions. For example, the immobile ions have

decreased from 87.2% to 85.3% at 550K, and 92.4% to 88.6% at 460K, respectively. The result shows that poly(C_2MTMA) has much shorter strings but fewer longer strings than poly(C_2VIm) at each simulated temperature. The statistics of the average string length $\langle n_S \rangle$ also shows the obviously shorter strings for poly(C_2MTMA) than poly(C_2VIm), where $\langle n_S \rangle$ varies from about 1.1 to 1.3 for the former in the temperature range of 460 to 570K, and 1.4 to 1.7 for the latter, respectively. In short, the long linker in poly(C_2MTMA) enables the smoother ion motion with shorter average string length, and in turn, the higher diffusivity when compared with poly(C_2VIm).

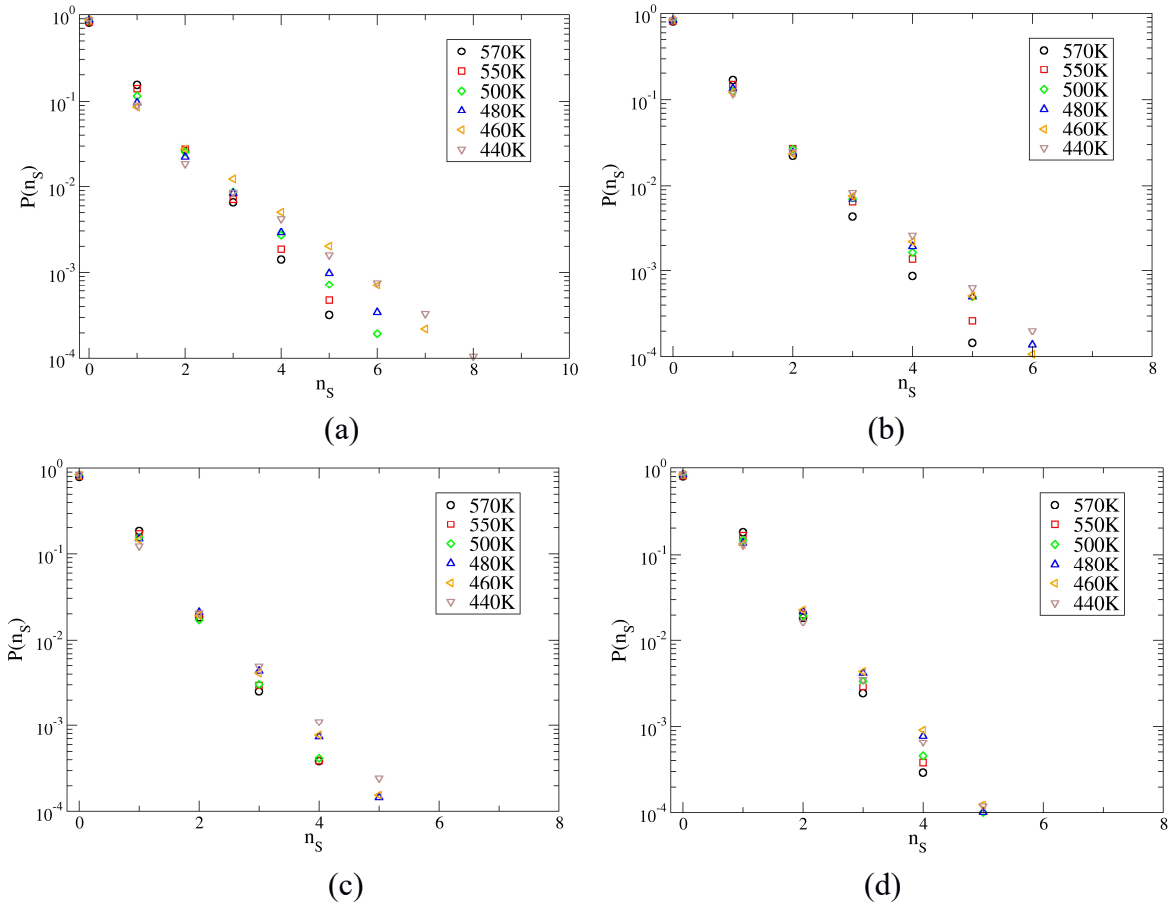

Figure 25. String length distribution of the cooperative motion for poly(CnMTMA) Tf2N as a function of temperature. (a) C1; (b) C2; (c) C4; (d) C5

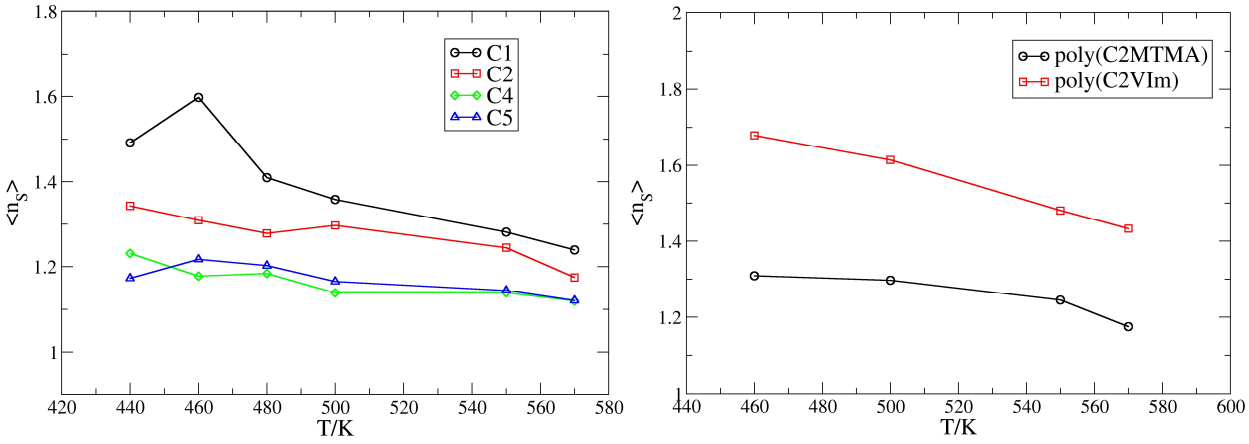

Figure 26. Left: Comparison of the average string length for poly(C_nMTMA) Tf2N with pendant tails of C1, C2, C4 and C5. Right: Comparison of the average string length for poly(C_2MTMA) and poly(C_2VIm).

References

[1] H. Liu, S.J. Paddison, Direct Comparison of Atomistic Molecular Dynamics Simulations and X-ray Scattering of Polymerized Ionic Liquids, ACS Macro Lett. 5 (2016) 537–543. doi:10.1021/acsmacrolett.6b00061.

[2] H. Liu, S.J. Paddison, Alkyl Chain Length Dependence of Backbone-to-Backbone Distance in Polymerized Ionic Liquids: An Atomistic Simulation Perspective on Scattering, Macromolecules. 50 (2017) 2889–2895. doi:10.1021/acs.macromol.6b02708.

[3] X. Luo, H. Liu, S.J. Paddison, Molecular dynamics simulations of polymerized ionic liquids: mechanism of ion transport for different anions, ACS Appl. Polym. Mater. Under revi (2020) ap-2020-00834t.

[4] L.M. Hall, M.J. Stevens, A.L. Frischknecht, Effect of Polymer Architecture and Ionic Aggregation on the Scattering Peak in Model Ionomers, Phys. Rev. Lett. 106 (2011) 127801. doi:10.1103/PhysRevLett.106.127801.

[5] L.M. Hall, M.E. Seitz, K.I. Winey, K.L. Opper, K.B. Wagener, M.J. Stevens, A.L. Frischknecht, Ionic Aggregate Structure in Ionomer Melts: Effect of Molecular Architecture on Aggregates and the Ionomer Peak, J. Am. Chem. Soc. 134 (2012) 574–587. doi:10.1021/ja209142b.

[6] J.A. Bollinger, M.J. Stevens, A.L. Frischknecht, Quantifying Single-Ion Transport in

Percolated Ionic Aggregates of Polymer Melts, ACS Macro Lett. 9 (2020) 583–587. doi:10.1021/acsmacrolett.0c00139.

[7] H. Liu, X. Luo, A.P. Sokolov, S.J. Paddison, Quantitative Evidence of Mobile Ion Hopping in Polymerized Ionic Liquids, J. Phys. Chem. B. Under revi (2020) jp-2020-06916q.

[8] C. Donati, J.F. Douglas, W. Kob, S.J. Plimpton, P.H. Poole, S.C. Glotzer, Stringlike cooperative motion in a supercooled liquid, Phys. Rev. Lett. 80 (1998) 2338–2341. doi:10.1103/PhysRevLett.80.2338.

[9] C. Donati, S.C. Glotzer, P.H. Poole, W. Kob, S.J. Plimpton, Spatial correlations of mobility and immobility in a glass-forming Lennard-Jones liquid, Phys. Rev. E. 60 (1999) 3107–3119. doi:10.1103/PhysRevE.60.3107.

[10] T. Pal, M. Vogel, On the relevance of electrostatic interactions for the structural relaxation of ionic liquids: A molecular dynamics simulation study, J. Chem. Phys. 150 (2019) 124501. doi:10.1063/1.5085508.

[11] S. Mogurampelly, J.R. Keith, V. Ganesan, Mechanisms Underlying Ion Transport in Polymerized Ionic Liquids, J. Am. Chem. Soc. 139 (2017) 9511–9514. doi:10.1021/jacs.7b05579.